Contract # 958007
Doc. # 9950-1375

FINAL REPORT

The 7 - 23 Micron Spectra of Extended Sources and Cirrus
NASA JPL 958007 (1989)

The 7 - 23 Micron Spectra of Infrared Cirrus
NASA JPL 958007 (1988)

SADAP Studies of the 7 to 23-Micron Spectrum of Infrared Cirrus
NASA JPL 958007 (1987)

David K. Lynch
John A. Hackwell
Space and Environment Technology Center
The Aerospace Corporation
P.O. Box 92957
Los Angeles, CA 90009

ATR 91(7176)-1

Table of Contents



This report was prepared for the Jet Propulsion Laboratory, California Institute of Technology, sponsored by the National Aeronautics and Space Administration.

# I. Introduction

Much of the energy emitted by cool objects in the Universe is in the infrared part of the spectrum, between roughly one micron and one millimeter. Most of this region can not be observed from the ground. The Infrared Astronomical Satellite (IRAS) surveyed 96% of the sky at 12, 25 60 and 100 μm in 1983-1984. One of the major discoveries made by the IRAS sensors was the infrared cirrus (Low et al. 1984), faint wisps of dust that appear to fill the galaxy.

The spacecraft also carried the Low Resolution Spectrograph (LRS), an instrument that obtained spectra of sources between 7.7 and 22 μm (Olnon and Raimond 1986). Because it was slitless, the LRS spectra are convolved with the spatial extent of the source. While the spectra of point sources experienced no degradation, the spectra of extended sources, especially those extended by many arc minutes, suffered severe loss of spectral resolution. In the case of most extended objects their spectra were useless.

Yet if the spatial structure of the source could be recovered, and if the spectral structure of the source did not change significantly as a function of position within the source, then there is a chance that the smeared spectra can be deconvolved from the spatial structure to yield the spectrum of the extended source with some if not all of its spectral resolution restored. With this goal in mind, we set about to recover the spectra of bright extended sources. The ultimate goal was to obtain spectra of the infrared cirrus.

This report describes the effort and results of these studies.

## 2. Approach to the Problem

The basic problem was to take the raw LRS data and use information from the survey scans of the sky to deconvolve spectra of extended objects. In order to do this, the spatial structure in the in-scan direction must be obtained. This information came from the IRAS 12 and 25 μm survey. Unfortunately, the survey detectors were not aligned with the five LRS detectors (LRS detectors 1, 2, and 3 spanned 7.7 - 13.4 μm, 4 and 5 covered 12 - 23 μm). Therefore when the focal plane scanned the sky (Figure 1) the survey detectors scanned different parts of the sky than did the LRS detectors. Even if the survey detectors were aligned with those of the LRS, the intrinsic spectral variation across the source could render any spectral recovery meaningless. While there was (and is) no a priori reason to believe that all sources are spectrally invariant across their extent, some certainly are. The recognition of this possibility was crucial to successful deconvolution. Therefore we tentatively assumed that, to first order, the sources we were preparing to analyze were spectrally invariant. This would allow us to develop our algorithms and techniques so that at a later date when we undertook to deconvolve cirrus spectra (cirrus probably is spectrally invariant), we would have the tools and knowledge available to proceed. We also recognized the need to co-add spectra of many cirrus filaments in order to achieve a useful signal to noise ratio.

The first step was to acquire the LRS data. At the time we began the project, no one was working on the LRS raw data and it was stored on magnetic tape at the Infrared Processing and Analysis Center (IPAC) in Pasadena. The raw data were required for analysis rather than the LRS data base (several thousand sources selected for scrutiny for inclusion in the LRS catalog) because the LRS catalog contained only those spectra from a small number of point sources. Once in hand, the nineteen tapes were sent to co-investigators Dr. Paul Wesselius of the Space Research Organization of Netherlands (SRON) in Groningen. Dr. Wesselius and his organization were chosen because they originally built the LRS and were in the best possible position to analyze data from it.

In Holland the raw data were unpacked from the tapes and placed on hard disk. They were then sorted scan by scan according to position on the sky. The Boresite Pointing History File (BPHF) was similarly parsed before being merged with the raw data. Selected sources were extracted from the data base before being sent to The Aerospace Corporation for analysis. The data used was the 12 and 25 μm scans, the LRS scans, the BPHF and other housekeeping information. Because the RA and dec were used only to select the regions and not to tag the data set, only time in spacecraft clock units was available. Furthermore, the dispersion in the prisms resulted in a wavelength calibration that was not only a nonlinear function of time, but also suffered from zero-clamping (Raimond, Beintema and Wesselius 1985) and digitization errors. These will be discussed more fully below.

The software necessary to accomplish the recovery was generated at The Aerospace Corporation. It was built around a maximum entropy algorithm (MEMSYS) developed by Gull and Skilling (1984). This software package was being used on another related ADP (then SADAP) program headed by Dr. John Hackwell at Aerospace for two-dimensional image deconvolution.

Progress was slow, owing to the severe computational and storage needs at SRON/Groningen. With people on two continents working their side of the problem, we managed, towards the end of the first year, to sit down with raw time-ordered data and begin the process of deconvolution.

## 3. Computational techniques

In order to deconvolve the spectral structure of extended sources from their spatial structure, some estimate of the spatial morphology must be made. Because the 12 μm survey data was close to the mid point of the LRS's wavelength range (7.7 - 22.8 μm), we used the 12 μm survey data as a guide to the spatial structure of the sources. The in-scan paths of the 12 μm survey detectors, however, did not coincide with those of the LRS survey detectors. It was therefore necessary to make some assessment of the source's spatial structure as it would be seen by a 12 μm detector whose path matched that of the LRS detector whose spectrum is to be deconvolved. This was accomplished by reconstructing a 12 μm image from the survey detectors and then extracting from it the

intensity profiles that matched the LRS detector paths.

To reconstruct the 12 μm image, the 12 μm raw survey detector data was obtained from the Space Research Organization of the Netherlands in Groningen in a 1 degree by 1 degree box centered on the source's nominal position. The data were rotated by the average angle between all of the scan legs and the in-scan direction of the focal plane so that the scans lay in the x-direction of the focal plane coordinate system, thereby insuring that all tails in the data due to detector hysteresis were pointing in the same direction. The data were despiked and destriped to remove relative detector level changes. Moshir's point response functions were applied to the data in preparation for the deconvolution. The deconvolution algorithm and software package were based on those of Gull and Skilling (1984) in their maximum entropy code as modified by Hackwell et al. (1988) for unequally spaced data.

The deconvolution process required an estimate of the noise for each data point in the image. We used two different noise estimators. The first was simply a constant fraction of the signal $\sigma_s$. Although $\sigma_s$ is not a true noise estimate, it was a necessary addition to the final noise estimate in order to limit the signal-to-noise ratio of the data in the unlikely event that the other noise estimators were zero. Because the signal varied at each point, so did $\sigma_s$. The second noise estimator was the standard deviation of the first difference of the scan data $\sigma_d$. This provided a realistic value of the average noise in the signal. $\sigma_d$ was a single number that was applied to each point in the data array. We calculated the final noise estimate $\sigma$ where $\sigma^2 = \sigma_d^2 + \sigma_s^2$.

An image recovery was then begun with an attempt to converge on a solution gridded on to a 7.5 arc sec by 60 arc sec regularly spaced grid. In maximizing the entropy and therefore the smoothness of the restored image, the software attempted to make the convolution of the restored image with the detectors' PSFs match to within the noise constraint specified above. Each unevenly sampled data point was associated with the nearest position on the regularly spaced grid when mapping between the raw data and the recovered image spaces. Instead of convolving the recovered image with the appropriate detector PSF in frequency space, the convolution was carried out directly with the mapping between data and image space handled simultaneously. This was necessary because of the unevenly sampled raw data which do not allow an efficient fast-fourier transform to be applied.

The progress of the deconvolution was monitored by examining the number of iterations necessary to converge and if it was successful, the quality of the recovered image was judged both qualitatively by eye as well as by noting the behavior of several critical chi-squared parameters as the algorithm approached its final solution. Successful convergence was deemed complete when the final image (Figure 2a) met the above criteria and when the image was insensitive to small changes in the noise multipliers. It was sometimes necessary to apply near-unity multipliers to both noise estimators in order to achieve convergence.

After the image was recovered, a two-dimensional strip that matched the path of the LRS detector was extracted from the image and integrated in the cross-scan direction to give the spatial profile (kernel) which was to be deconvolved with the LRS data. It was then multiplied by the cross-scan response of the appropriate LRS detector so that the intensity variation of the source registered by the LRS detector could be simulated as closely as possible. The kernel was trimmed to remove extraneous sources of background noise and to make the background level of the wings as similar as possible. The minimum value was subtracted to insure that the model was positive definite but not on a pedestal. The kernel was padded with zeros so that its centroid was within one pixel of the center to avoid shifting the final spectrum by less than one pixel during recovery; this also defined the mid-point of the kernel as a wavelength calibration point. Finally the area under the kernel was normalized to unity (Figure 2b) in preparation for deconvolution with the raw LRS spectrum (Figure 2c).

In addition to the two above-mentioned noise estimators, a third one was added to the raw LRS data, our so-called gradient noise $\sigma_G$. $\sigma_G$ was defined as the 1st derivative of the LRS data and was necessary to account for uncertainties in the wavelength calibration. Like $\sigma_s$, $\sigma_G$ was an array. $\sigma_G$ was added in quadrature with $\sigma_d$ and $\sigma_s$ to give $\sigma$, the final noise estimator. As before, near-unity multipliers were occasionally used to achieve convergence or to test the stability of the solution. The deconvolution was performed and convergence was monitored and judged successful (Figure 2d) according to criterion similar to those for the image recovery.

The deconvolved spectrum calculated by MEMSYS lacked error bars: the code had no way of generating them internally. Therefore the only way we were able to assess the reality of spectral features was to vary the noise estimates and monitor the stability of the solution. In most cases the results were robust and solid.

The most stable spectra did not seem to have spectral resolution as high as those of point sources. Attempt to increase the spectral resolution resulted in a chaos-like behavior: spectral features would split in two, then each peak would split again, etc. The results were unreasonable and unstable.

Flux calibration was done by performing the same set of operations on our calibration star $\alpha$ Tau. The resulting raw processed spectrum of $\alpha$ Tau was divided into the recovered spectrum of the source and then multiplied by the flux model of $\alpha$ Tau. We used as our flux model a 3000 K black body scaled to -3.01 magnitudes at N (10.2 $\mu$m), or $1.87 \times 10^{-15}$ W $cm^{-1}$ $\mu m^{-1}$ . Wavelength calibration was performed by looking at known lines in spectra of planetary nebulae and verified by noting the known turn-on and turn off wavelengths of the short- and long-wavelength LRS signals. Since the optical properties of the focal plane and LRS were known, the wavelength calibration generated at SRON was also used as a check of our own.

## 4. Results on selected Bright Extended Sources

Figures 2d, 3, 4 and 5 show the deconvolved spectra of IC 4637, NGC 2023, NGC 2024 and the Crab nebula. Only NGC 2023 has a ground-based spectrum in the IR region covered by the LRS and those observations were made with such a small beam as to make any comparison of little value. Experiments with the MEMSYS package revealed that the overall shapes of the continua are probably correct but the strength and location of the emission features are dependent on the noise estimators and therefore may not be real.

## 5. Discussion

The most difficult aspect of interpreting the results was this: despite the assurances based on numerous tests that the MEMSYS was providing the correct answer within the framework of chi-squared and maximum entropy, there was no way to be certain that the results were physically meaningful. There were no test cases for which we knew the answers. Most of the sources we were studying were 2 - 6 arc minutes across, far too large for any kind of ground based spectroscopy except with the smallest of telescopes (12" diameter or less).

Particularly troublesome to deconvolve, i.e. those whose final spectra were most sensitive to the noise estimators, were sources whose spectra had a low signal to noise ratio. We were not able to make much progress with these faint extended sources. Specifically, only a few regions such as Orion and R CrA had cirrus bright enough to show up in the raw LRS spectra. This work will continue under the NASA sponsored study The 7 - 23 μm LRS Spectra of Comet Trails and Comae, Contract NAS5-30793, D.

K. Lynch, Principal Investigator.

## 6. Summary and Outlook

LRS spectra of selected extended objects have been deconvolved with their reconstructed 12 μm spatial profiles. The resulting spectra show spectral structure that is not present in the processed data. The continuum shapes are thought to be correct but the accuracy of the line structure is uncertain. We are continuing to develop the technique for extended objects and comets, and the results will be reported at the end of our second contract "The 7 - 23 μm LRS Spectra of Comet Trails and Comae".

## 7. Acknowledgements

We would like to acknowledge the contributions to this program made by Rob Olling, Pjotr Roelfsema, Peter Arendz, Thijs de Graauw, Thije de Young, David Edelsohn, Stephan Mazuk, Elizabeth Walkup and Peter Erwin.

8. References

Gull, S.F. and Skilling, J., 1984, IEE Proc., 131, Pt. F., No. 6, 646.

Hackwell, J.A., Friesen, L. M., Canterna, R. and Grasdalen, G.L., 1988, B.A.A.S., 26, 677.

Low, F.J. et al., 1984, Ap. J. (Lett.), 278, L19.

Lynch, D.K., Hackwell, J.A., Wesselius, P., Olling, R., and Israel, F., 1988, "IRAS LRS Spectra of Extended Sources," B.A.A.S., 20, No. 2, 732, 172nd Meeting of the A.A.S., Kansas City, June 5-9, 1988.

Olnon, F.M., and Raimond, E., "IRAS Catalogs and Atlases. Atlas of Low Resolution Spectra", Astr. and Ap. (Suppl.), 65, 607 (1986).

Raimond, E., Beintema, D.A. and Wesselius, P.R., 1985, in IRAS Catalogs and Atlases - Explanatory Supplement, C. A. Beichman et al., Ed.

Figure Captions

Figure 1 IRAS Focal Plane

Figure 2a Recovered 12 μm image of IC 4637

2b Deconvolution kernel obtained from 12 μm image ( 2a)

2c LRS data

2d Spectrum obtained by deconvolving 2b with 2c

Figure 3 Deconvolved spectrum of NGC 2023

Figure 4 Deconvolved spectrum of NGC 2024

Figure 5 Deconvolved spectrum of the Crab Nebula

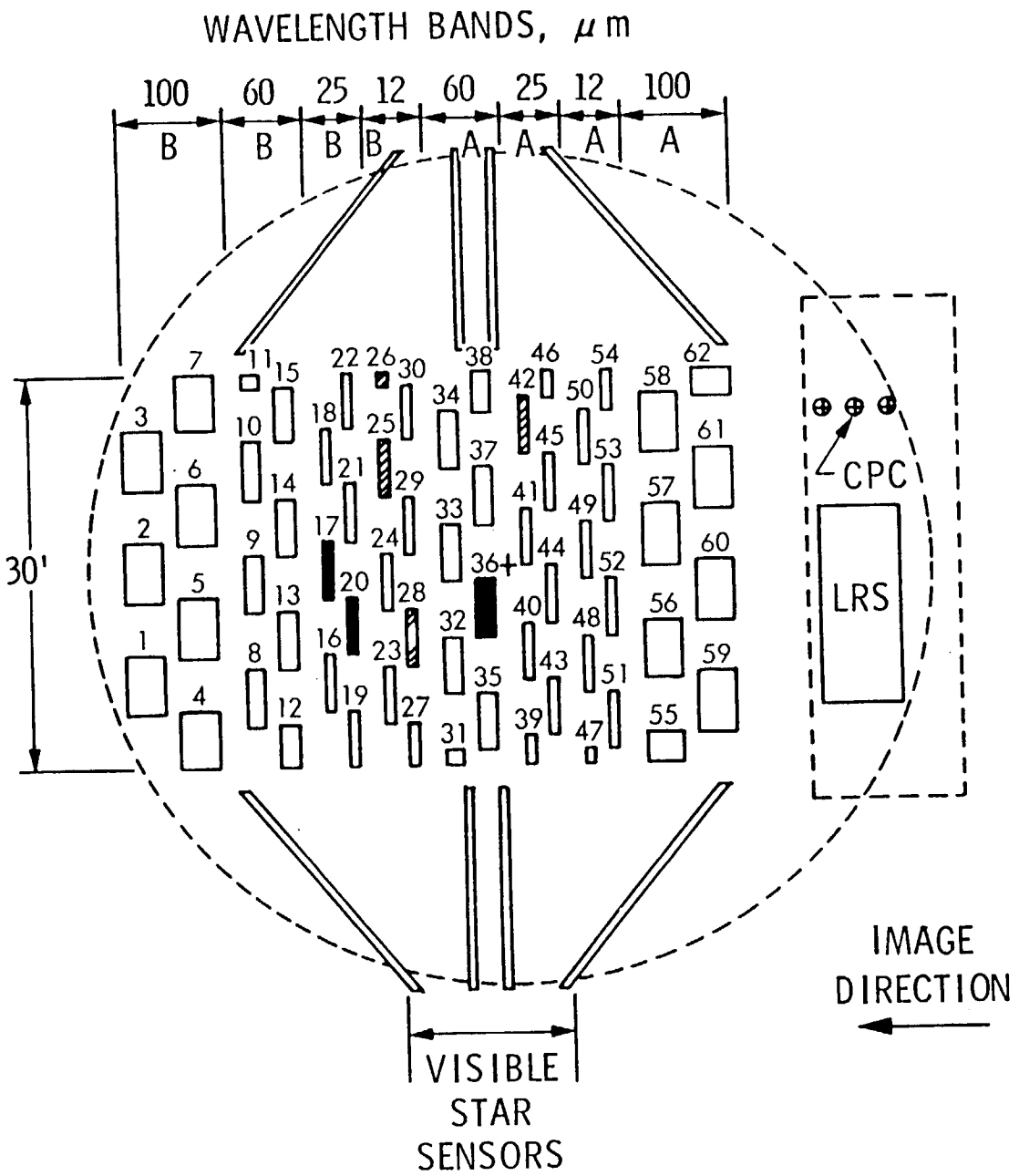
WAVELENGTH BANDS, μm
100
60
25
12
60
25
12
100
B
B
B
B
A
A
A
A
30'
CPC
LRS
IMAGE
DIRECTION
VISIBLE
STAR
SENSORS

Figure 1

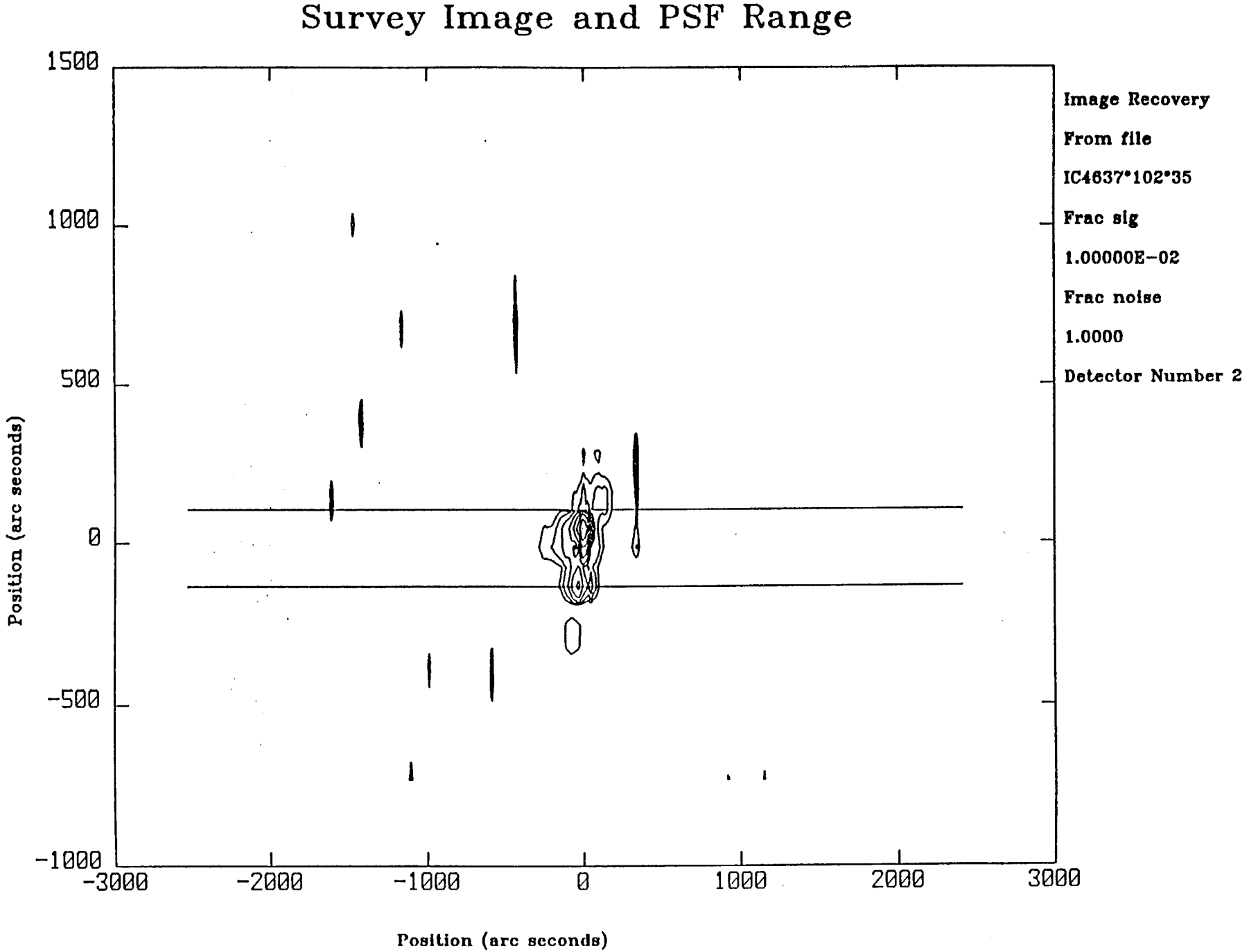
Survey Image and PSF Range
1500
1000
500
0
-500
-1000
-3000
-2000
-1000
0
1000
2000
3000
Position (arc seconds)
Position (arc seconds)
Image Recovery
From file
IC4637*102*35
Frac sig
1.00000E-02
Frac noise
1.0000
Detector Number 2

Figure 2a

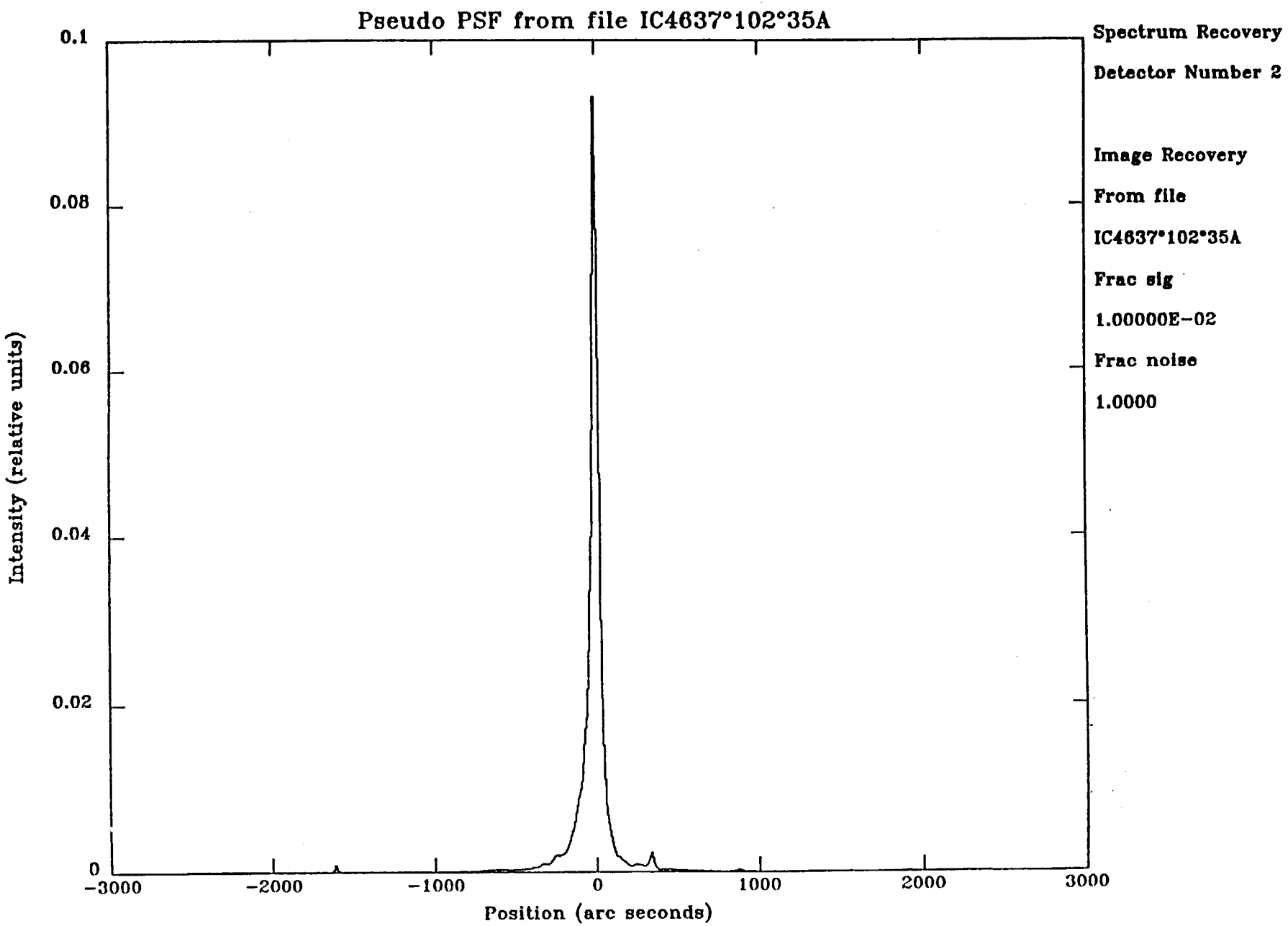
Pseudo PSF from file IC4637°102°35A
Spectrum Recovery
Detector Number 2
Image Recovery
From file
IC4637°102°35A
Frac sig
1.00000E-02
Frac noise
1.0000
Intensity (relative units)
0.1
0.08
0.06
0.04
0.02
0
−3000
−2000
−1000
0
1000
2000
3000
Position (arc seconds)

Figure 2b

No overflow

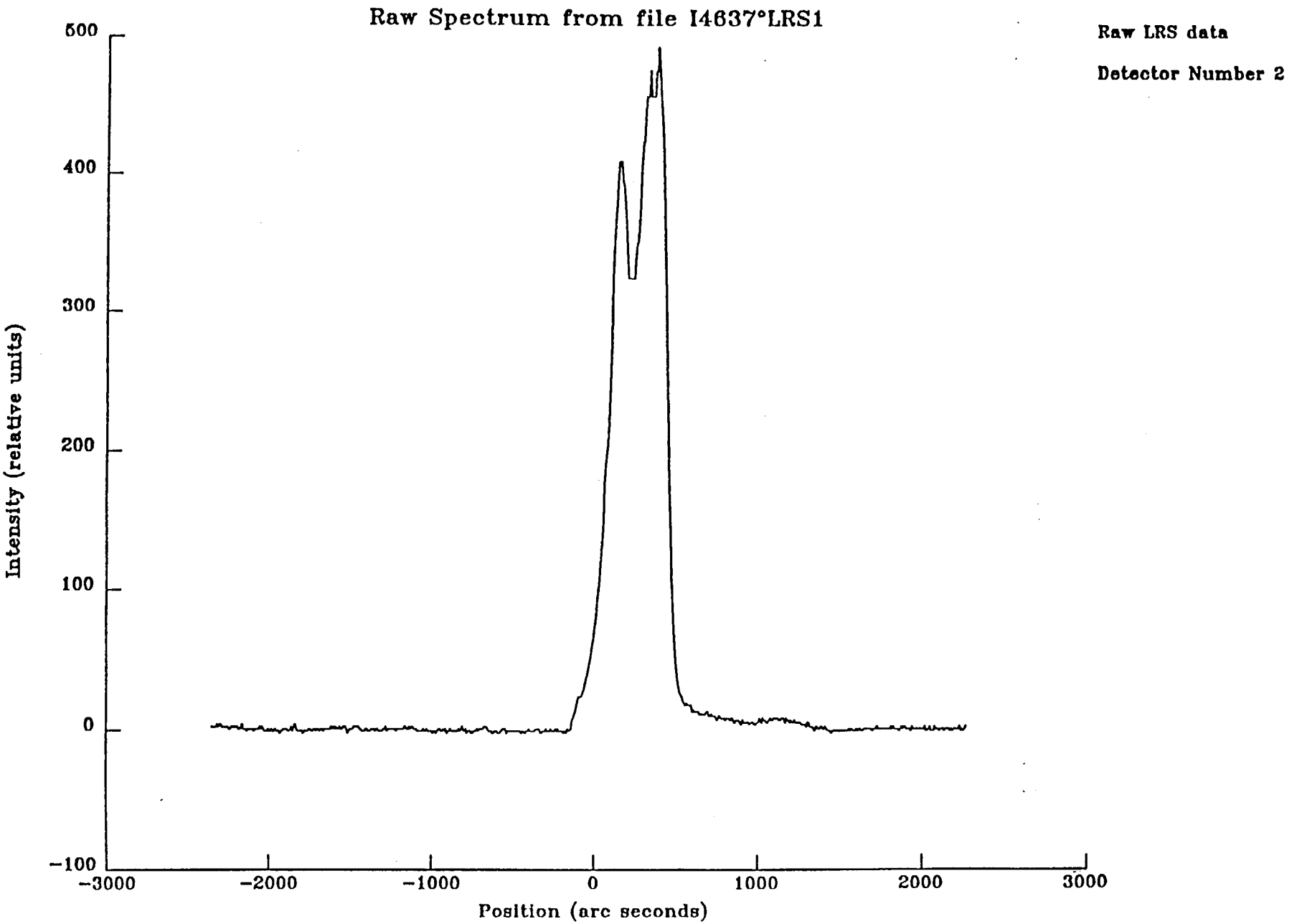


Figure 2c

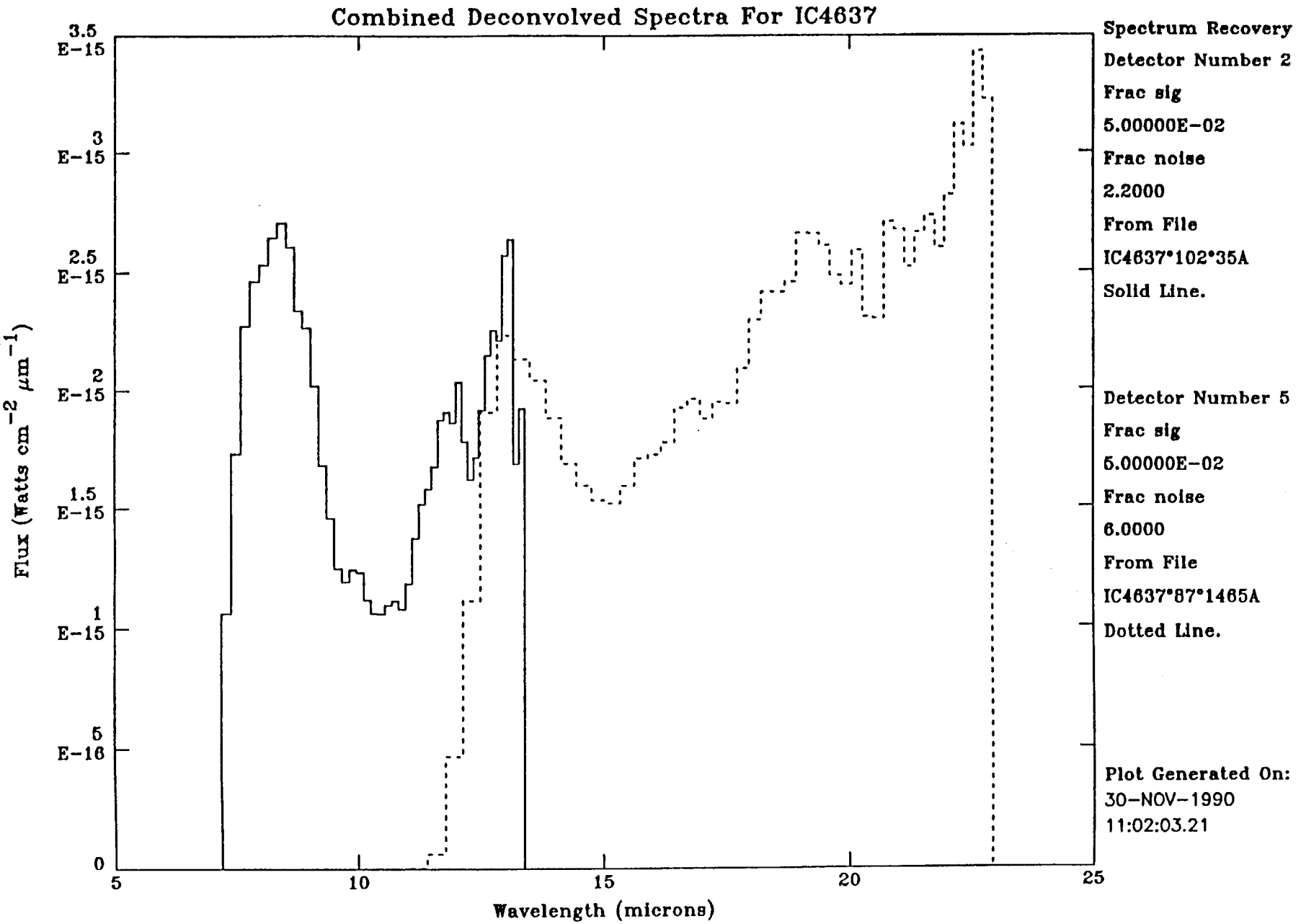
Combined Deconvolved Spectra For IC4637
Flux (Watts cm$^{-2}$ $\mu$m$^{-1}$)
3.5 E-15
3 E-15
2.5 E-15
2 E-15
1.5 E-15
1 E-15
5 E-16
0
5
10
15
20
25
Wavelength (microns)
Spectrum Recovery
Detector Number 2
Frac sig
5.00000E-02
Frac noise
2.2000
From File
IC4637°102°35A
Solid Line.
Detector Number 5
Frac sig
5.00000E-02
Frac noise
6.0000
From File
IC4637°87°1465A
Dotted Line.
Plot Generated On:
30-NOV-1990
11:02:03.21

Figure 2d

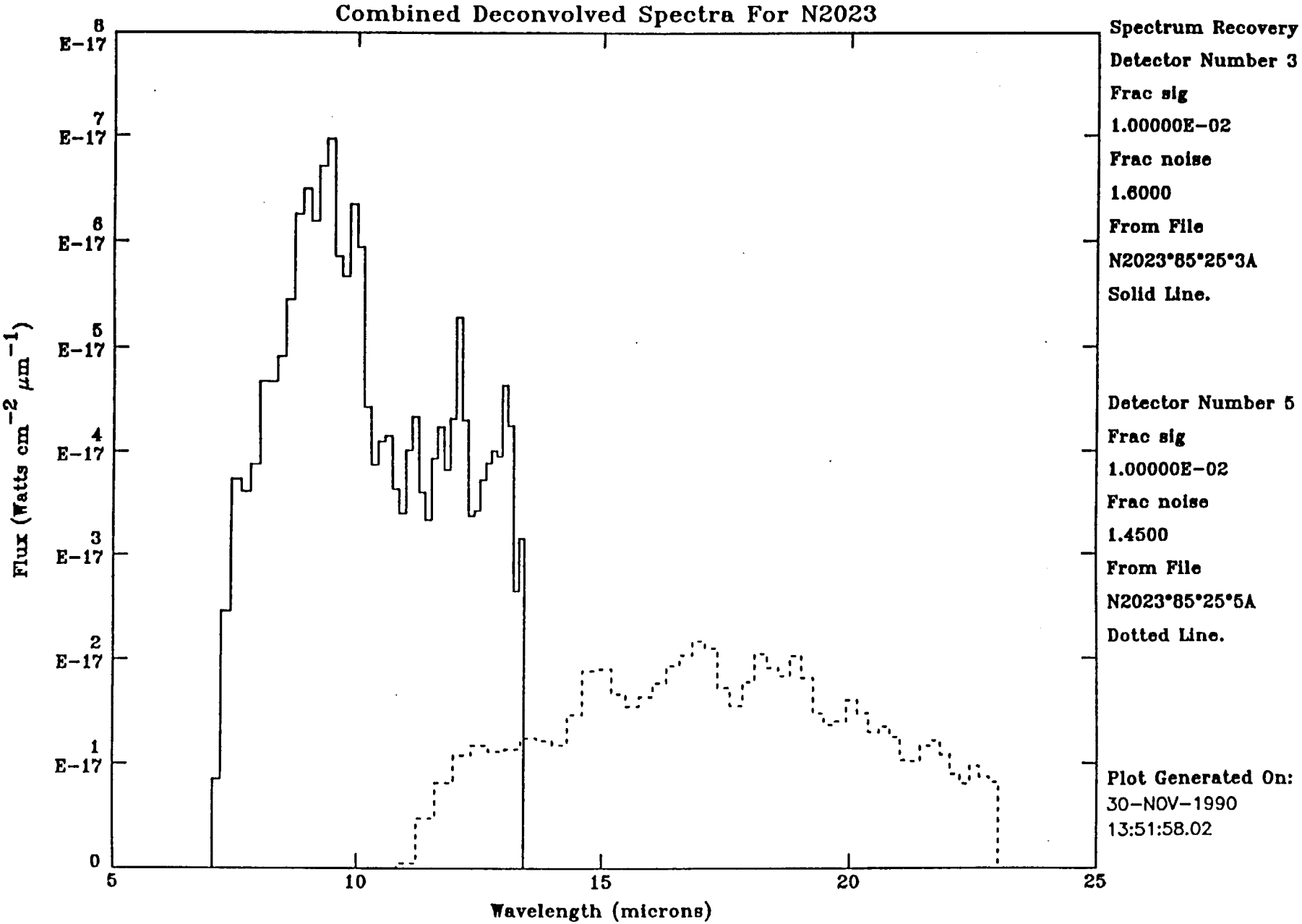
Combined Deconvolved Spectra For N2023
Flux (Watts cm$^{-2}$ μm$^{-1}$)
8 E-17
7 E-17
6 E-17
5 E-17
4 E-17
3 E-17
2 E-17
1 E-17
0
5
10
15
20
25
Wavelength (microns)
Spectrum Recovery
Detector Number 3
Frac sig
1.00000E-02
Frac noise
1.6000
From File
N2023°85°25°3A
Solid Line.
Detector Number 5
Frac sig
1.00000E-02
Frac noise
1.4500
From File
N2023°85°25°5A
Dotted Line.
Plot Generated On:
30-NOV-1990
13:51:58.02

Figure 3

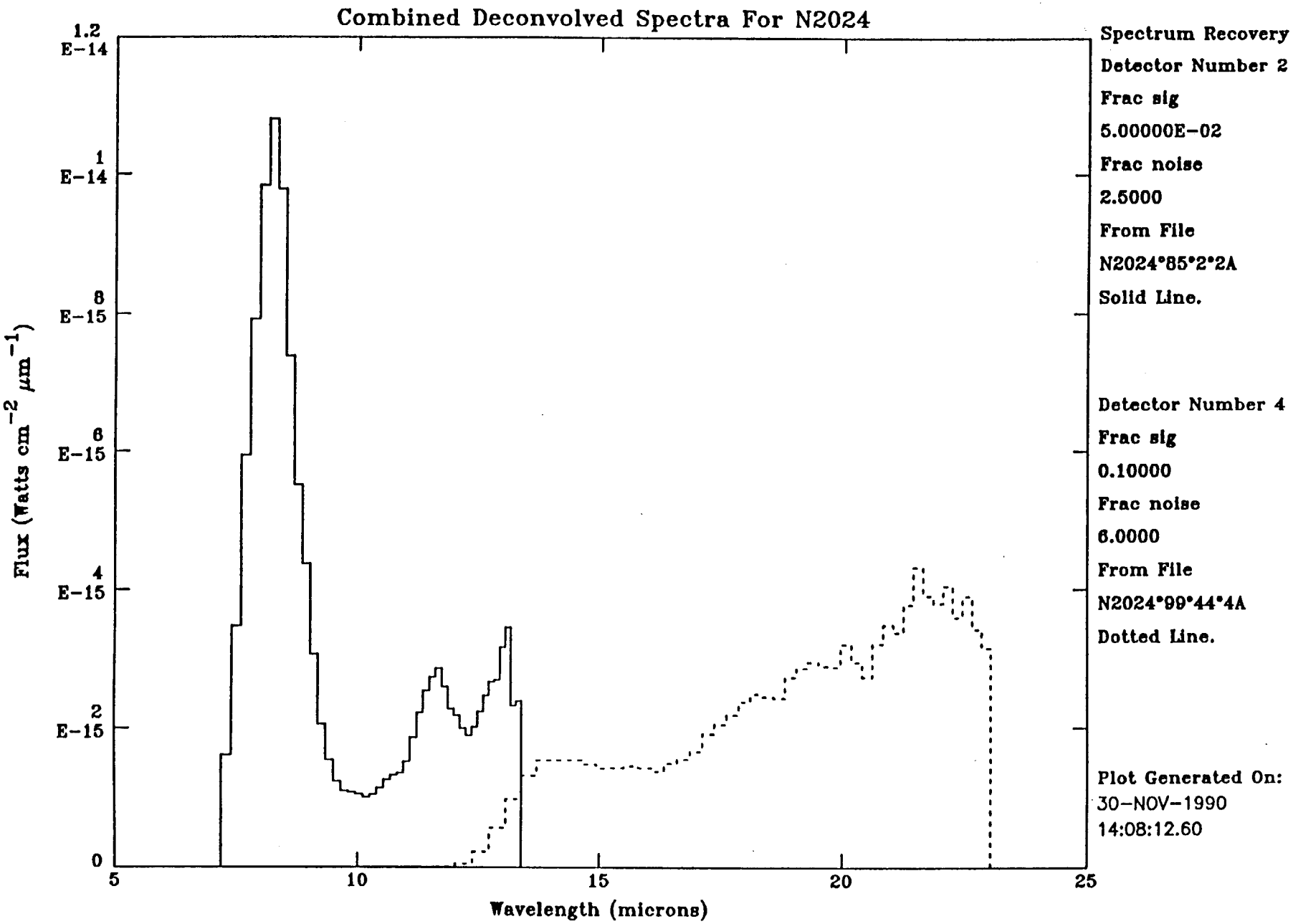
Combined Deconvolved Spectra For N2024
Flux (Watts cm$^{-2}$ μm$^{-1}$)
1.2 E-14
1 E-14
8 E-15
6 E-15
4 E-15
2 E-15
0
5
10
15
20
25
Wavelength (microns)
Spectrum Recovery
Detector Number 2
Frac sig
5.00000E-02
Frac noise
2.5000
From File
N2024*85*2*2A
Solid Line.
Detector Number 4
Frac sig
0.10000
Frac noise
6.0000
From File
N2024*99*44*4A
Dotted Line.
Plot Generated On:
30-NOV-1990
14:08:12.60

Figure 4

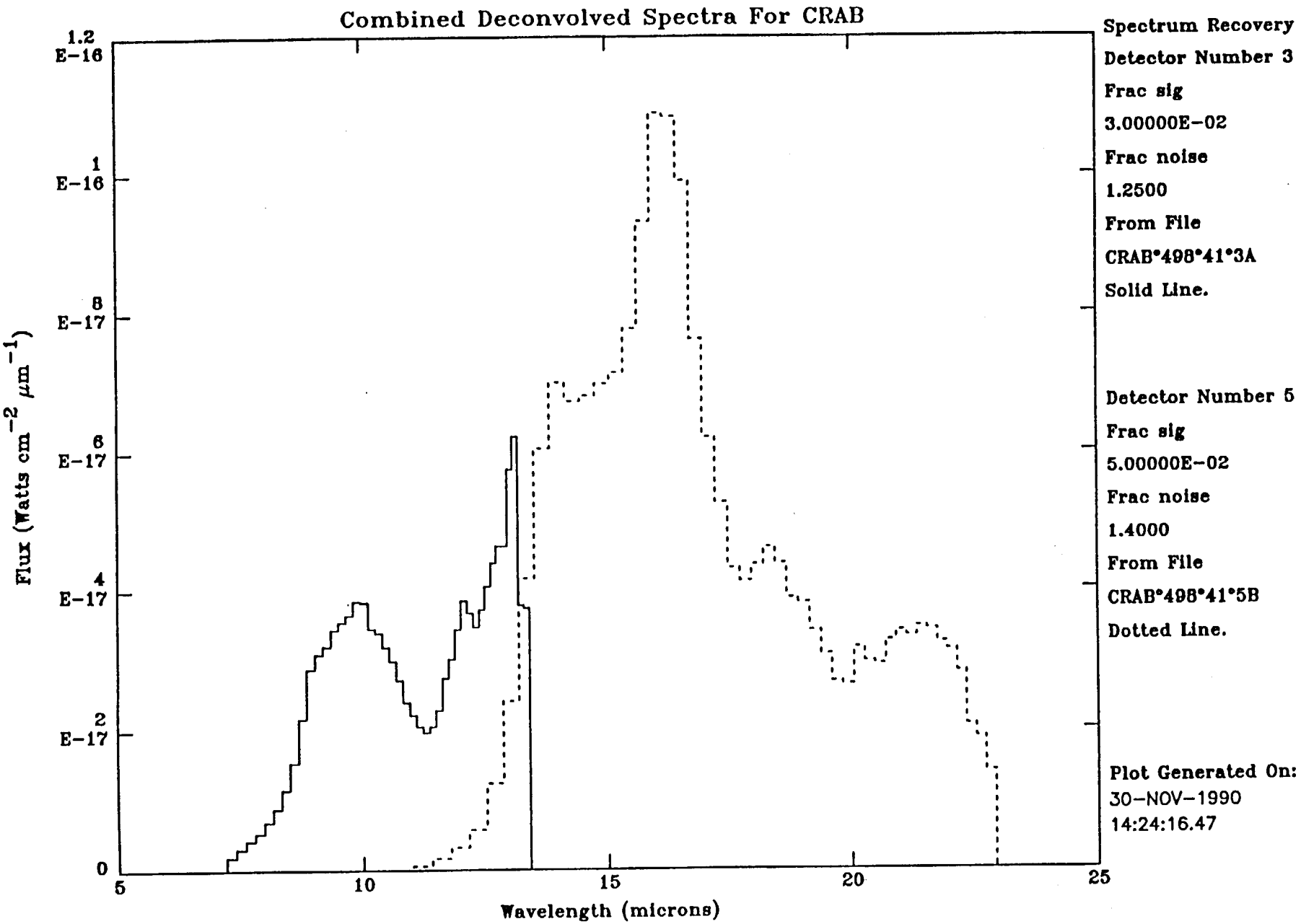
Combined Deconvolved Spectra For CRAB
Flux (Watts cm$^{-2}$ $\mu$m$^{-1}$)
1.2 E-16
1 E-16
8 E-17
6 E-17
4 E-17
2 E-17
0
5
10
15
20
25
Wavelength (microns)
Spectrum Recovery
Detector Number 3
Frac sig
3.00000E-02
Frac noise
1.2500
From File
CRAB°498°41°3A
Solid Line.
Detector Number 5
Frac sig
5.00000E-02
Frac noise
1.4000
From File
CRAB°498°41°5B
Dotted Line.
Plot Generated On:
30-NOV-1990
14:24:16.47

Figure 5

Appendix I.

# IRAS LRS Spectra of Extended Objects: The Crab Nebula"

by

Lynch, D. K., Hackwell, J. A., Edelsohn, D. J., Wesselius, P., Olling, R., and Israel, F. P.

Proceedings of the 22nd Eslab Symposium on Infrared Spectroscopy in Astronomy,

M. Kessler, (Ed.), SP-290, 193-195, Dec. 7-9, 1988, Salamanca, Spain.

# IRAS LRS SPECTRA OF EXTENDED OBJECTS: THE CRAB NEBULA

**D K Lynch, J A Hackwell, D J Edelsohn,**
Space Sciences Laboratory, The Aerospace Corporation,
P.O. Box 92957, Los Angeles, CA 90009

**P Wesselius, R Olling,**
Laboratory for Space Research of the National Institute for Space Research,
Groningen, The Netherlands

**F P Israel**
Huygens Laboratory, University of Leiden, The Netherlands

## 1. ABSTRACT/RESUME

We have recovered the spectra of extended sources from the raw Low Resolution Spectrometer (LRS) data by means of a nonlinear deconvolution technique built around a maximum entropy algorithm. The results are applied to the Crab Nebula, a supernova remnant extended by about 4 arc minutes. The deconvolved spectrum of the Crab shows significant departures from a blackbody spectrum, with emission features present at 10.2, 11.3, 12.3 and 12.8 μm.

## 2. INTRODUCTION

One of the most unexpected discoveries made by IRAS was the pervasive low-contrast filamentary emission that is commonly called "infrared cirrus" (Low et al. 1984). The cirrus, which is most obvious on the 100 μm sky brightness images, extends to high galactic latitudes and is unevenly distributed over most of the sky. The emission is from interstellar dust that is heated both locally and by the diffuse galactic radiation field, but the composition and size distribution of the dust grains are unknown.

The Low Resolution Spectrograph (LRS) on board the IRAS satellite produced a continuous stream of raw spectral data as the satellite scanned the sky (Raimond et al. 1985). Processing of the raw data involved the extraction of any spectrum which correlated with sources from the Point Source Catalog (PSC) or any other known point source. A point source was defined by practical convention to be a source less than about 40 seconds of arc in diameter. The resulting LRS data base was further winnowed based on the number of observations, the 12 and 25 μm fluxes and other "goodness" tests. The resulting LRS Catalog, (Olnon and Raimond 1986) though substantive and reliable, is not complete for it excludes bright sources observed only once (e.g. Betelgeusc), sources from the Small Scale Structure Catalog (Helou and Walker, 1985) and other extended sources (e.g. HII regions), certain emission line objects with weak continua, any object whose 12 and 25 μm brightness was less than 1 and 2 Jy respectively, and most of the cirrus.

The LRS was a slitless spectrograph. In such instruments both spectral and spatial structure are convolved with one another. The point spread function for point sources is so closely approximated by a delta function that the convolved spectrum is indistinguishable from the unconvolved spectrum. For extended sources, however, the ability to recover the true spectrum requires having the in-scan spatial profile of the source which must be deconvolved from the observed spectrum. Obtaining the in-scan profile and using it to deconvolved the observed (raw) spectrum is a major goal of this program.

In this paper we shall describe our efforts toward extracting 7-23 μm spectra of infrared cirrus from the unpublished raw LRS data stream and to expand our studies to include other extended (2-6 arc minutes) objects.

## 3. DATA RETRIEVAL AND SOFTWARE TECHNIQUES

The software techniques necessary to reconstruct LRS spectra of faint and extended sources were developed under a NASA SADAP/ADP program. While many important refinements remain to be implemented, the core of the software is complete. Several steps are required (Figure 1) and we shall explain the technique by showing the short wavelength results from the Crab Nebula, a 34 Jy (at 12 μm) supernova remnant that is extended by about 4 arc minutes:

I. The LRS data and survey data are extracted from the raw data tapes as one degree fields around the source of interest and integrated with the boresight pointing history file. This is done at SRON/Groningen using software developed specifically for this program.

II. The 12 and 25 μm survey data scans are gridded onto sky plates using the point response functions of each individual detector. A destriped image of the source is generated using a maximum entropy image restoration system developed around Gull and Skilling's algorithm (Gull and Skill 1984; Hackwell et al. 1988). The reconstructed image of the Crab Nebula is shown in Figure 1a. The accuracy of this vital

*Proc. 22nd Eslab Symposium on Infrared Spectroscopy in Astronomy, Salamanca, Spain, 7-9 December 1988, ESA SP-290 (September 1989)*

step was proven by the fact that higher spatial resolution images of the Crab obtained from the Additional Observations (AOs) showed precisely the same structure seen in Figure 1a.

III. The reconstructed image (Figure 1a) is then sliced up along the in-scan direction and a "pseudo 12 μm survey scan" is generated (Figure 1b) whose path across the source precisely matches the path taken by the LRS detector(s). In this way, cross scan spectral structure that was scanned by the LRS but not necessarily scanned by any single survey detector is included in a deconvolution function, called the point spread function, or PSF.

IV. The pseudo-survey scan (Figure 1b) is used as the deconvolution function for the raw data (Figure 1c) to generate the uncalibrated deconvolved spectrum (Figure 1d). This is also done using the maximum entropy system, a nonlinear restoration algorithm which is able to achieve results unobtainable using conventional linear techniques.

The system shown has not been divided by the flux calibrator. However, an examination of the raw spectra of the calibrators shows them to be smooth, monotonically decreasing (with wavelength) functions with no spectral structure. Thus we believe the spectral features in Figure 1d are real, and not artifacts.

We have developed the software tools necessary to do this job, as shown in the above example on the Crab Nebula. In addition to the Crab, we have also recovered some of the spectra from the highly extended HII region NGC 2024 (Lynch et al. 1988) and the extended reflection nebula NGC 2023. Recent experience suggests that spectra with signal-to-noise ratios of about 10 can be extracted for sources with a 12 μm flux of 5-10 Jy. For cirrus sources which are generally fainter than 1 Jy at 12 μm, we will have to co-add hundreds of spectra in order to produce spectra with sufficient signal-to-noise to identify spectral features.

We wish to emphasis the importance of these extractions: it is now possible to obtain an LRS spectrum of any location in the sky, including sources not found in the point source catalog, the LRS catalog or the LRS data base. There are limitations of the technique as well. The deconvolution process assumes at the outset that there are no variations in spectral structure from one part of the source to another (e.g., blackbody on the north end and emission lines on the south). While such variations are no doubt present to some extent in any source, we must be aware that we cannot detect or correct for such effects.

## 4. SPECTRUM OF THE CRAB

It is clear from Figure 1d that the spectrum of the Crab departs strongly from that of a blackbody. Four emission features are present with wavelengths near 10.2, 11.3, 12.3 and 12.8 μm, respectively. Systematic uncertainties in the wavelength calibration presently limit the accuracy of wavelength identification to ± 0.3 μm. The spectral resolution of our techniques is strongly dependent on the intrinsic signal-to-noise ratio of the source and, in the case of the Crab, we have not resolved the emission features in Figure 1d.

We believe the feature at 12.8 μm is due to [Ne II]. The identities of the features at 10.2, 11.3 and 12.3 μm are not yet known. We cannot yet tell whether they are atomic line emission that is not resolved or broadband dust emission features that are nearly or totally resolved.

## 5. CONCLUSION

Techniques now exist for recovering spectra of extended objects from the raw LRS data using a nonlinear deconvolution technique. Results so far indicate that a number of highly extended objects including the Crab Nebula show emission line features which cannot be observed from the ground.

## 6. ACKNOWLEDGEMENTS

This work was supported by NASA Grant No. JPL 958007 and the Aerospace Sponsored Research Program.

## 7. REFERENCES

1. Gull, S.F. and Skilling, J., 1984, IEE Proc., 131, Pt. F., No. 6, 646.

2. Hackwell, J.A., Friesen, L. M., Canterna, R. and Grasdalen, G.L., 1988, B.A.A.S., 26, 677.

3. Low, F.J. et al., 1984, Ap. J. (Lett.), 278, L19.

4. Lynch, D.K., Hackwell, J.A., Wesselius, P., Olling, R., and Israel, F., 1988, "IRAS LRS Spectra of Extended Sources," B.A.A.S., 20, No. 2, 732, 172nd Meeting of the A.A.S., Kansas City, June 5-9, 1988.

5. Olnon, F.M., and Raimond, E., 1986, Astr. and Ap. (Suppl.), 65, 607.

6. Raimond, E., Beintema, D.A. and Wesselius, P.R., 1985, in IRAS Catalogs and Atlases - Explanatory Supplement, C. A. Beichman et al., Ed.

## 8. FIGURE CAPTIONS

1a. Image of the Crab Nebula reconstructed from 12 μm IRAS survey scans. Note structure, which also appears in higher resolution images obtained at 12 μm using Additional Observations (AO) data. The path taken by detector #2 across the source is shown by the two parallel lines.

1b. In-scan slice from the reconstructed image above (Figure 1a) whose width exactly matches the cross scan width of the LRS detector number 2. This scan is the point spread function (PSF) used to deconvolved the raw spectrum (Figure 1c).

1c. Raw LRS data for detector 2 crossing the Crab Nebula. The spectral structure is convolved with the spatial structure.

1d. Final short wavelength spectrum of the Crab obtained by deconvolving Figure 1b with Figure 1c using the nonlinear maximum entropy system.

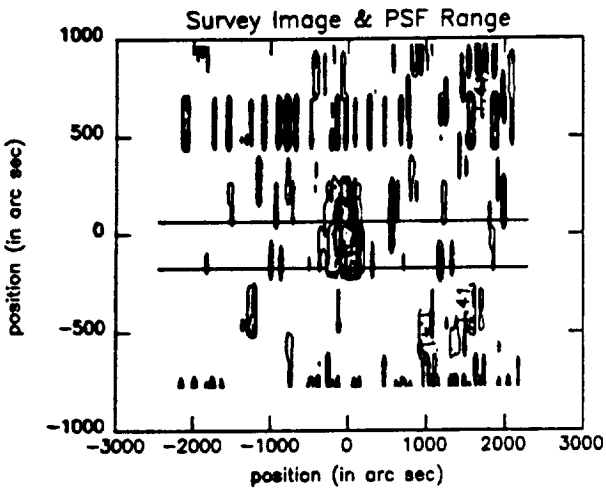


Figure 1a

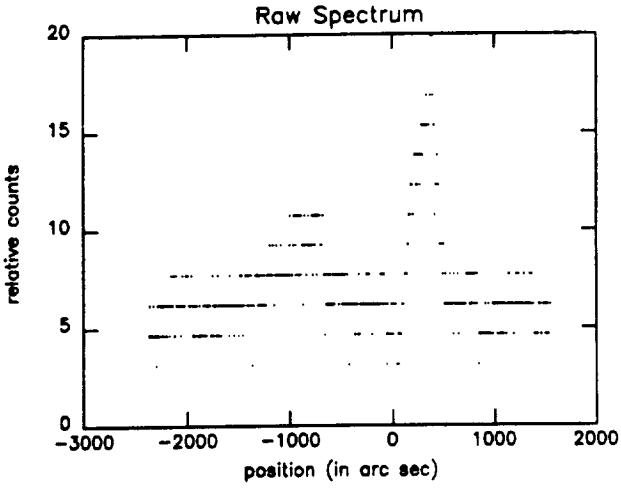


Figure 1c

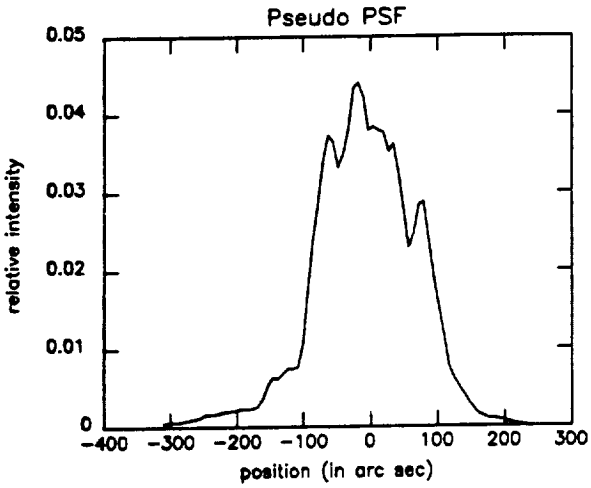


Figure 1b

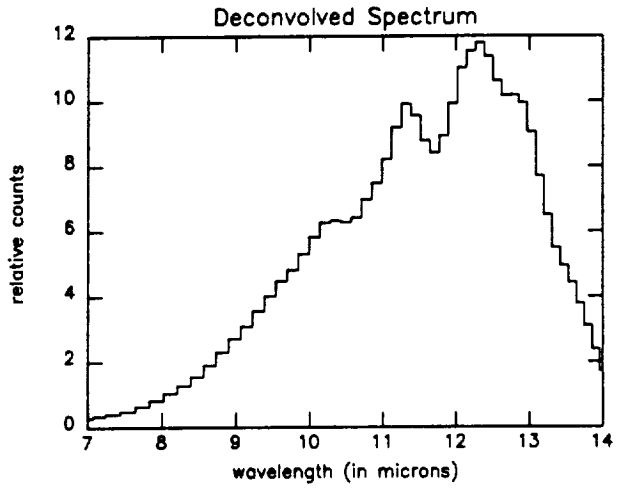


Figure 1d

Contract # 958007
Document # 9950-1375

FINAL REPORT

The 7 - 23 Micron Spectra of Extended Sources and Cirrus
NASA JPL 958007 (1989)

The 7 - 23 Micron Spectra of Infrared Cirrus
NASA JPL 958007 (1988)

SADAP Studies of the 7 to 23-Micron Spectrum of Infrared Cirrus
NASA JPL 958007 (1987)

David K. Lynch
John A. Hackwell
Space and Environment Technology Center
The Aerospace Corporation
P.O. Box 92957
Los Angeles, CA 90009

ATR 91(7176)-1

Table of Contents



This report was prepared for the Jet Propulsion Laboratory, California Institute of Technology, sponsored by the National Aeronautics and Space Administration.

# I. Introduction

Much of the energy emitted by cool objects in the Universe is in the infrared part of the spectrum, between roughly one micron and one millimeter. Most of this region can not be observed from the ground. The Infrared Astronomical Satellite (IRAS) surveyed 96% of the sky at 12, 25 60 and 100 μm in 1983-1984. One of the major discoveries made by the IRAS sensors was the infrared cirrus (Low et al. 1984), faint wisps of dust that appear to fill the galaxy.

The spacecraft also carried the Low Resolution Spectrograph (LRS), an instrument that obtained spectra of sources between 7.7 and 22 μm (Olnon and Raimond 1986). Because it was slitless, the LRS spectra are convolved with the spatial extent of the source. While the spectra of point sources experienced no degradation, the spectra of extended sources, especially those extended by many arc minutes, suffered severe loss of spectral resolution. In the case of most extended objects their spectra were useless.

Yet if the spatial structure of the source could be recovered, and if the spectral structure of the source did not change significantly as a function of position within the source, then there is a chance that the smeared spectra can be deconvolved from the spatial structure to yield the spectrum of the extended source with some if not all of its spectral resolution restored. With this goal in mind, we set about to recover the spectra of bright extended sources. The ultimate goal was to obtain spectra of the infrared cirrus.

This report describes the effort and results of these studies.

## 2. Approach to the Problem

The basic problem was to take the raw LRS data and use information from the survey scans of the sky to deconvolve spectra of extended objects. In order to do this, the spatial structure in the in-scan direction must be obtained. This information came from the IRAS 12 and 25 μm survey. Unfortunately, the survey detectors were not aligned with the five LRS detectors (LRS detectors 1, 2, and 3 spanned 7.7 - 13.4 μm, 4 and 5 covered 12 - 23 μm). Therefore when the focal plane scanned the sky (Figure 1) the survey detectors scanned different parts of the sky than did the LRS detectors. Even if the survey detectors were aligned with those of the LRS, the intrinsic spectral variation across the source could render any spectral recovery meaningless. While there was (and is) no a priori reason to believe that all sources are spectrally invariant across their extent, some certainly are. The recognition of this possibility was crucial to successful deconvolution. Therefore we tentatively assumed that, to first order, the sources we were preparing to analyze were spectrally invariant. This would allow us to develop our algorithms and techniques so that at a later date when we undertook to deconvolve cirrus spectra (cirrus probably is spectrally invariant), we would have the tools and knowledge available to proceed. We also recognized the need to co-add spectra of many cirrus filaments in order to achieve a useful signal to noise ratio.

The first step was to acquire the LRS data. At the time we began the project, no one was working on the LRS raw data and it was stored on magnetic tape at the Infrared Processing and Analysis Center (IPAC) in Pasadena. The raw data were required for analysis rather than the LRS data base (several thousand sources selected for scrutiny for inclusion in the LRS catalog) because the LRS catalog contained only those spectra from a small number of point sources. Once in hand, the nineteen tapes were sent to co-investigators Dr. Paul Wesselius of the Space Research Organization of Netherlands (SRON) in Groningen. Dr. Wesselius and his organization were chosen because they originally built the LRS and were in the best possible position to analyze data from it.

In Holland the raw data were unpacked from the tapes and placed on hard disk. They were then sorted scan by scan according to position on the sky. The Boresite Pointing History File (BPHF) was similarly parsed before being merged with the raw data. Selected sources were extracted from the data base before being sent to The Aerospace Corporation for analysis. The data used was the 12 and 25 μm scans, the LRS scans, the BPHF and other housekeeping information. Because the RA and dec were used only to select the regions and not to tag the data set, only time in spacecraft clock units was available. Furthermore, the dispersion in the prisms resulted in a wavelength calibration that was not only a nonlinear function of time, but also suffered from zero-clamping (Raimond, Beintema and Wesselius 1985) and digitization errors. These will be discussed more fully below.

The software necessary to accomplish the recovery was generated at The Aerospace Corporation. It was built around a maximum entropy algorithm (MEMSYS) developed by Gull and Skilling (1984). This software package was being used on another related ADP (then SADAP) program headed by Dr. John Hackwell at Aerospace for two-dimensional image deconvolution.

Progress was slow, owing to the severe computational and storage needs at SRON/Groningen. With people on two continents working their side of the problem, we managed, towards the end of the first year, to sit down with raw time-ordered data and begin the process of deconvolution.

## 3. Computational techniques

In order to deconvolve the spectral structure of extended sources from their spatial structure, some estimate of the spatial morphology must be made. Because the 12 μm survey data was close to the mid point of the LRS's wavelength range (7.7 - 22.8 μm), we used the 12 μm survey data as a guide to the spatial structure of the sources. The in-scan paths of the 12 μm survey detectors, however, did not coincide with those of the LRS survey detectors. It was therefore necessary to make some assessment of the source's spatial structure as it would be seen by a 12 μm detector whose path matched that of the LRS detector whose spectrum is to be deconvolved. This was accomplished by reconstructing a 12 μm image from the survey detectors and then extracting from it the

intensity profiles that matched the LRS detector paths.

To reconstruct the 12 μm image, the 12 μm raw survey detector data was obtained from the Space Research Organization of the Netherlands in Groningen in a 1 degree by 1 degree box centered on the source's nominal position. The data were rotated by the average angle between all of the scan legs and the in-scan direction of the focal plane so that the scans lay in the x-direction of the focal plane coordinate system, thereby insuring that all tails in the data due to detector hysteresis were pointing in the same direction. The data were despiked and destriped to remove relative detector level changes. Moshir's point response functions were applied to the data in preparation for the deconvolution. The deconvolution algorithm and software package were based on those of Gull and Skilling (1984) in their maximum entropy code as modified by Hackwell et al. (1988) for unequally spaced data.

The deconvolution process required an estimate of the noise for each data point in the image. We used two different noise estimators. The first was simply a constant fraction of the signal $\sigma_s$. Although $\sigma_s$ is not a true noise estimate, it was a necessary addition to the final noise estimate in order to limit the signal-to-noise ratio of the data in the unlikely event that the other noise estimators were zero. Because the signal varied at each point, so did $\sigma_s$. The second noise estimator was the standard deviation of the first difference of the scan data $\sigma_d$. This provided a realistic value of the average noise in the signal. $\sigma_d$ was a single number that was applied to each point in the data array. We calculated the final noise estimate $\sigma$ where $\sigma^2 = \sigma_d^2 + \sigma_s^2$.

An image recovery was then begun with an attempt to converge on a solution gridded on to a 7.5 arc sec by 60 arc sec regularly spaced grid. In maximizing the entropy and therefore the smoothness of the restored image, the software attempted to make the convolution of the restored image with the detectors' PSFs match to within the noise constraint specified above. Each unevenly sampled data point was associated with the nearest position on the regularly spaced grid when mapping between the raw data and the recovered image spaces. Instead of convolving the recovered image with the appropriate detector PSF in frequency space, the convolution was carried out directly with the mapping between data and image space handled simultaneously. This was necessary because of the unevenly sampled raw data which do not allow an efficient fast-fourier transform to be applied.

The progress of the deconvolution was monitored by examining the number of iterations necessary to converge and if it was successful, the quality of the recovered image was judged both qualitatively by eye as well as by noting the behavior of several critical chi-squared parameters as the algorithm approached its final solution. Successful convergence was deemed complete when the final image (Figure 2a) met the above criteria and when the image was insensitive to small changes in the noise multipliers. It was sometimes necessary to apply near-unity multipliers to both noise estimators in order to achieve convergence.

After the image was recovered, a two-dimensional strip that matched the path of the LRS detector was extracted from the image and integrated in the cross-scan direction to give the spatial profile (kernel) which was to be deconvolved with the LRS data. It was then multiplied by the cross-scan response of the appropriate LRS detector so that the intensity variation of the source registered by the LRS detector could be simulated as closely as possible. The kernel was trimmed to remove extraneous sources of background noise and to make the background level of the wings as similar as possible. The minimum value was subtracted to insure that the model was positive definite but not on a pedestal. The kernel was padded with zeros so that its centroid was within one pixel of the center to avoid shifting the final spectrum by less than one pixel during recovery; this also defined the mid-point of the kernel as a wavelength calibration point. Finally the area under the kernel was normalized to unity (Figure 2b) in preparation for deconvolution with the raw LRS spectrum (Figure 2c).

In addition to the two above-mentioned noise estimators, a third one was added to the raw LRS data, our so-called gradient noise $\sigma_G$. $\sigma_G$ was defined as the 1st derivative of the LRS data and was necessary to account for uncertainties in the wavelength calibration. Like $\sigma_s$, $\sigma_G$ was an array. $\sigma_G$ was added in quadrature with $\sigma_d$ and $\sigma_s$ to give $\sigma$, the final noise estimator. As before, near-unity multipliers were occasionally used to achieve convergence or to test the stability of the solution. The deconvolution was performed and convergence was monitored and judged successful (Figure 2d) according to criterion similar to those for the image recovery.

The deconvolved spectrum calculated by MEMSYS lacked error bars: the code had no way of generating them internally. Therefore the only way we were able to assess the reality of spectral features was to vary the noise estimates and monitor the stability of the solution. In most cases the results were robust and solid.

The most stable spectra did not seem to have spectral resolution as high as those of point sources. Attempt to increase the spectral resolution resulted in a chaos-like behavior: spectral features would split in two, then each peak would split again, etc. The results were unreasonable and unstable.

Flux calibration was done by performing the same set of operations on our calibration star $\alpha$ Tau. The resulting raw processed spectrum of $\alpha$ Tau was divided into the recovered spectrum of the source and then multiplied by the flux model of $\alpha$ Tau. We used as our flux model a 3000 K black body scaled to -3.01 magnitudes at N (10.2 $\mu$m), or $1.87 \times 10^{-15}$ W $cm^{-1}$ $\mu m^{-1}$ . Wavelength calibration was performed by looking at known lines in spectra of planetary nebulae and verified by noting the known turn-on and turn off wavelengths of the short- and long-wavelength LRS signals. Since the optical properties of the focal plane and LRS were known, the wavelength calibration generated at SRON was also used as a check of our own.

## 4. Results on selected Bright Extended Sources

Figures 2d, 3, 4 and 5 show the deconvolved spectra of IC 4637, NGC 2023, NGC 2024 and the Crab nebula. Only NGC 2023 has a ground-based spectrum in the IR region covered by the LRS and those observations were made with such a small beam as to make any comparison of little value. Experiments with the MEMSYS package revealed that the overall shapes of the continua are probably correct but the strength and location of the emission features are dependent on the noise estimators and therefore may not be real.

## 5. Discussion

The most difficult aspect of interpreting the results was this: despite the assurances based on numerous tests that the MEMSYS was providing the correct answer within the framework of chi-squared and maximum entropy, there was no way to be certain that the results were physically meaningful. There were no test cases for which we knew the answers. Most of the sources we were studying were 2 - 6 arc minutes across, far too large for any kind of ground based spectroscopy except with the smallest of telescopes (12" diameter or less).

Particularly troublesome to deconvolve, i.e. those whose final spectra were most sensitive to the noise estimators, were sources whose spectra had a low signal to noise ratio. We were not able to make much progress with these faint extended sources. Specifically, only a few regions such as Orion and R CrA had cirrus bright enough to show up in the raw LRS spectra. This work will continue under the NASA sponsored study The 7 - 23 μm LRS Spectra of Comet Trails and Comae, Contract NAS5-30793, D.

K. Lynch, Principal Investigator.

## 6. Summary and Outlook

LRS spectra of selected extended objects have been deconvolved with their reconstructed 12 μm spatial profiles. The resulting spectra show spectral structure that is not present in the processed data. The continuum shapes are thought to be correct but the accuracy of the line structure is uncertain. We are continuing to develop the technique for extended objects and comets, and the results will be reported at the end of our second contract "The 7 - 23 μm LRS Spectra of Comet Trails and Comae".

## 7. Acknowledgements

We would like to acknowledge the contributions to this program made by Rob Olling, Pjotr Roelfsema, Peter Arendz, Thijs de Graauw, Thije de Young, David Edelsohn, Stephan Mazuk, Elizabeth Walkup and Peter Erwin.

8. References

Gull, S.F. and Skilling, J., 1984, IEE Proc., 131, Pt. F., No. 6, 646.

Hackwell, J.A., Friesen, L. M., Canterna, R. and Grasdalen, G.L., 1988, B.A.A.S., 26, 677.

Low, F.J. et al., 1984, Ap. J. (Lett.), 278, L19.

Lynch, D.K., Hackwell, J.A., Wesselius, P., Olling, R., and Israel, F., 1988, "IRAS LRS Spectra of Extended Sources," B.A.A.S., 20, No. 2, 732, 172nd Meeting of the A.A.S., Kansas City, June 5-9, 1988.

Olnon, F.M., and Raimond, E., "IRAS Catalogs and Atlases. Atlas of Low Resolution Spectra", Astr. and Ap. (Suppl.), 65, 607 (1986).

Raimond, E., Beintema, D.A. and Wesselius, P.R., 1985, in IRAS Catalogs and Atlases - Explanatory Supplement, C. A. Beichman et al., Ed.

Figure Captions

Figure 1 IRAS Focal Plane

Figure 2a Recovered 12 μm image of IC 4637

2b Deconvolution kernel obtained from 12 μm image ( 2a)

2c LRS data

2d Spectrum obtained by deconvolving 2b with 2c

Figure 3 Deconvolved spectrum of NGC 2023

Figure 4 Deconvolved spectrum of NGC 2024

Figure 5 Deconvolved spectrum of the Crab Nebula

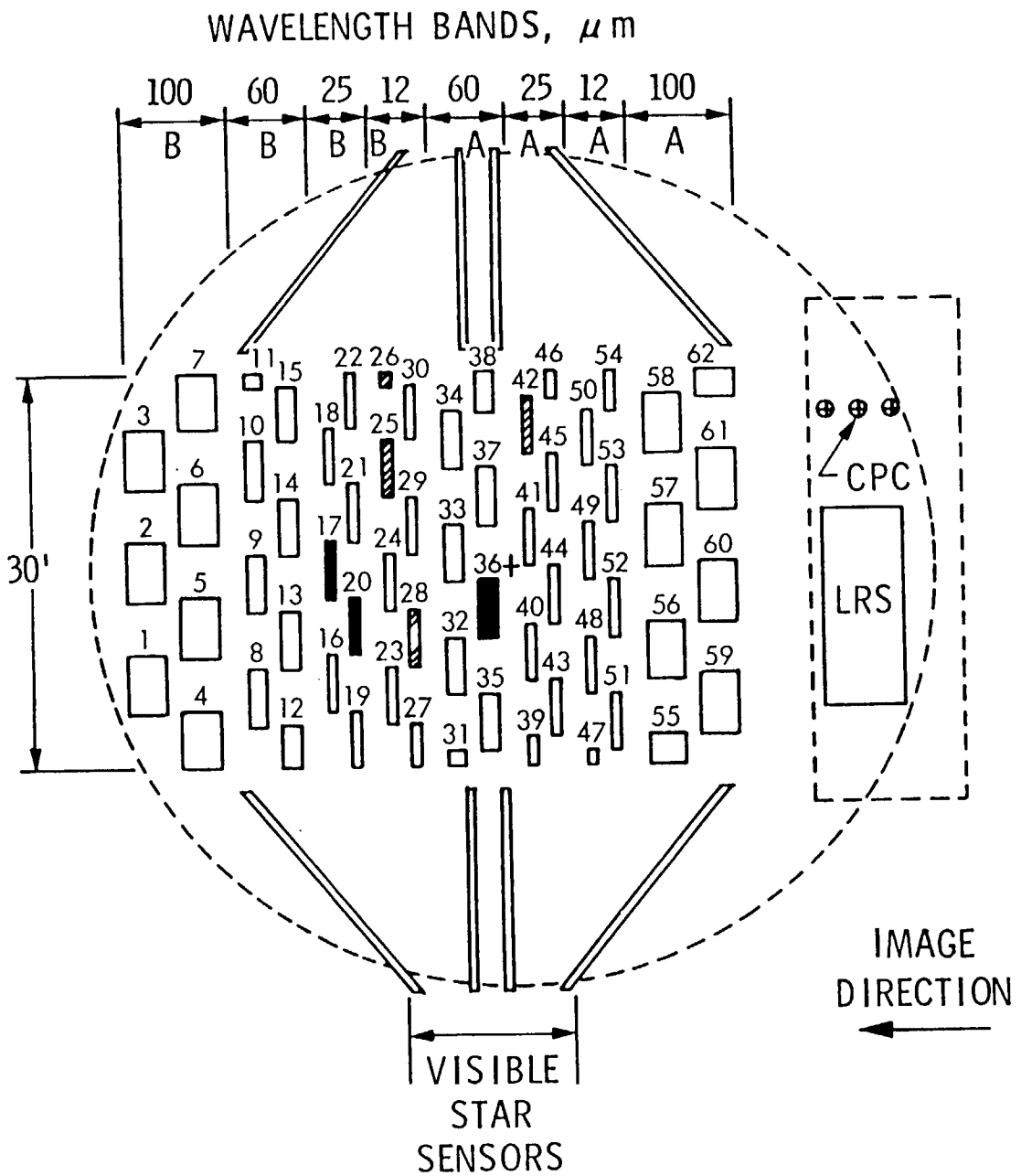
WAVELENGTH BANDS, μm
100
60
25
12
60
25
12
100
B
B
B
B
A
A
A
A
30'
CPC
LRS
IMAGE
DIRECTION
VISIBLE
STAR
SENSORS

Figure 1

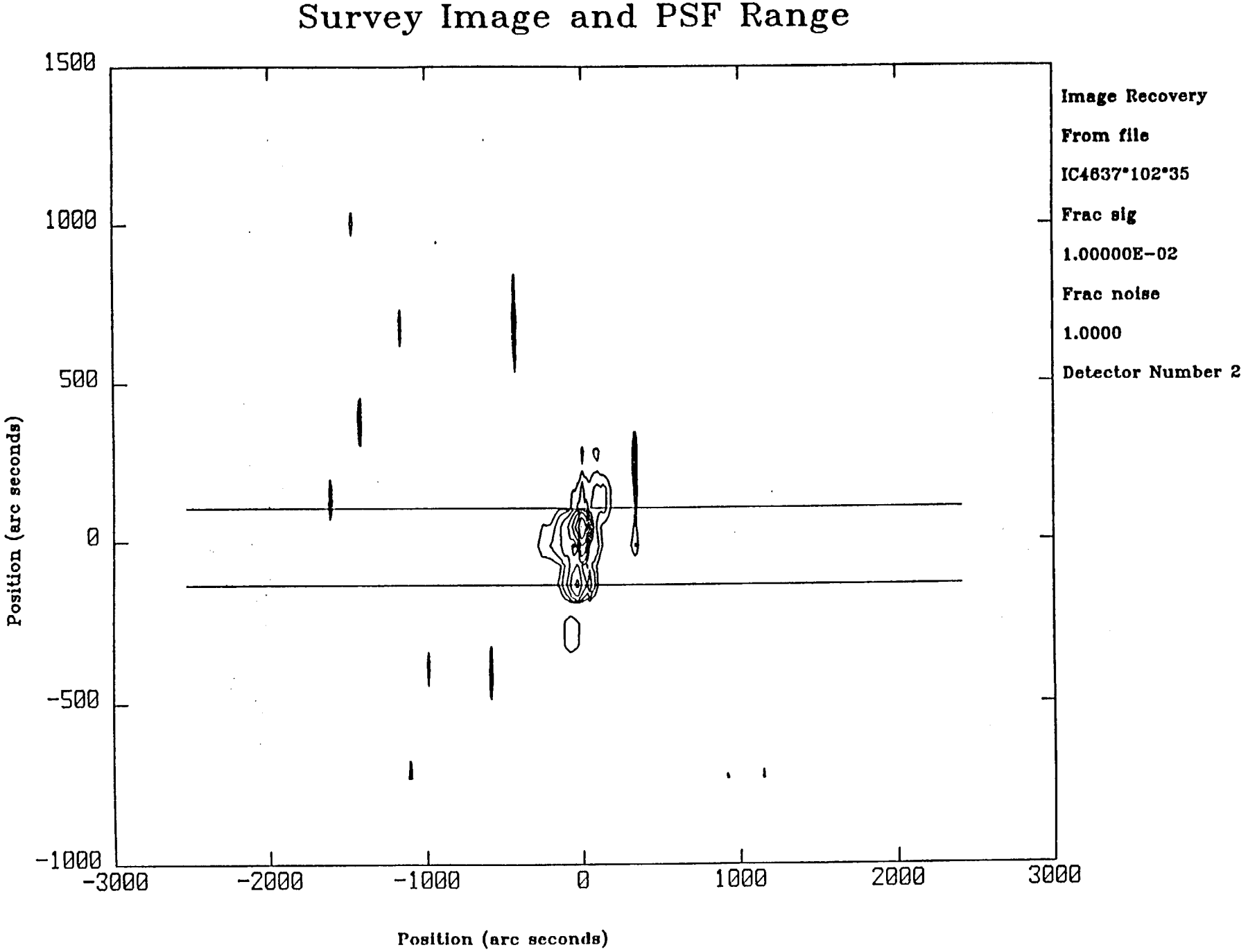
Survey Image and PSF Range
1500
1000
500
0
-500
-1000
-3000
-2000
-1000
0
1000
2000
3000
Position (arc seconds)
Position (arc seconds)
Image Recovery
From file
IC4637*102*35
Frac sig
1.00000E-02
Frac noise
1.0000
Detector Number 2

Figure 2a

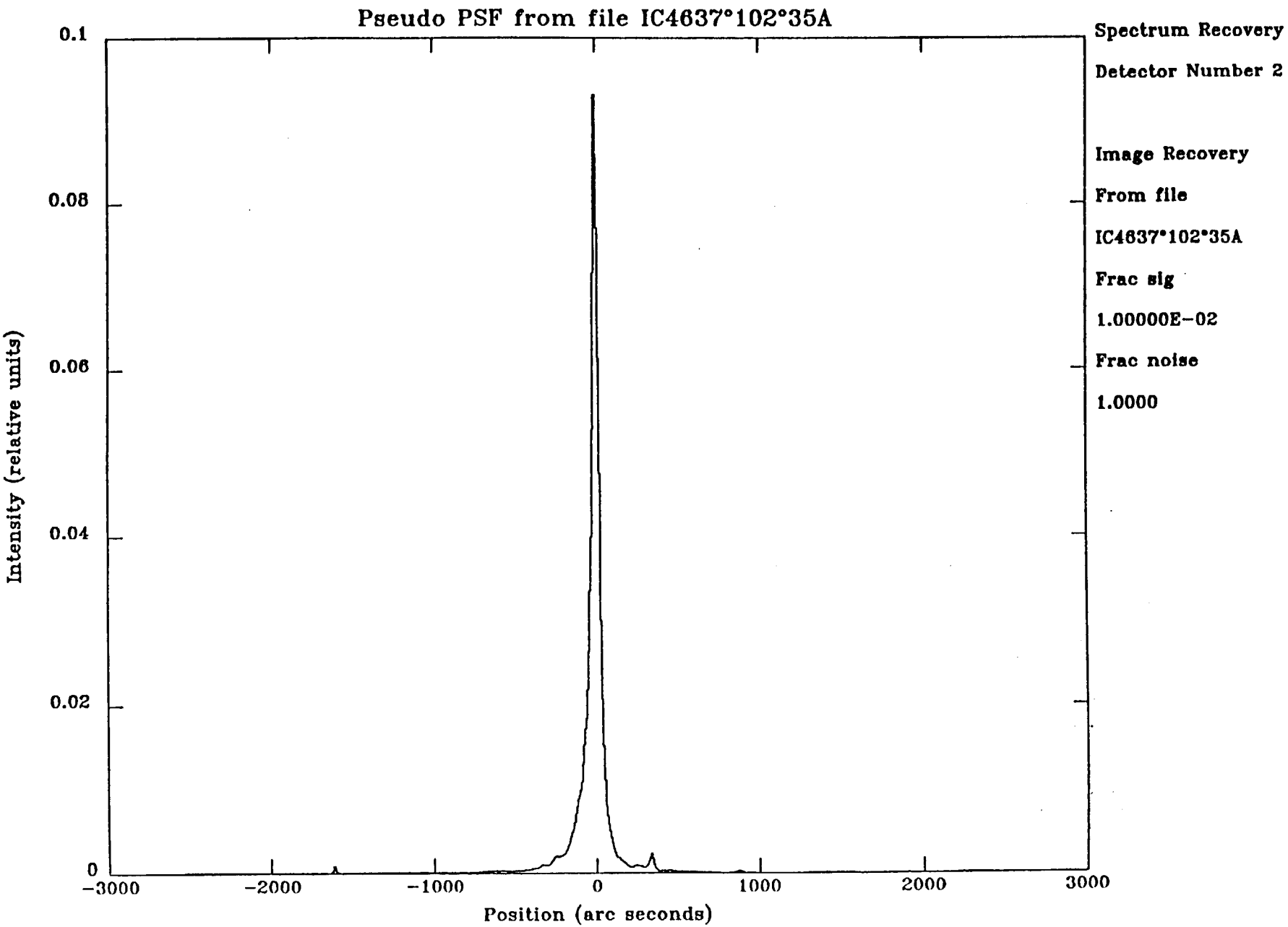
Pseudo PSF from file IC4637°102°35A
Spectrum Recovery
Detector Number 2
Image Recovery
From file
IC4637°102°35A
Frac sig
1.00000E-02
Frac noise
1.0000
Intensity (relative units)
0.1
0.08
0.06
0.04
0.02
0
−3000
−2000
−1000
0
1000
2000
3000
Position (arc seconds)

Figure 2b

No overflow. vv

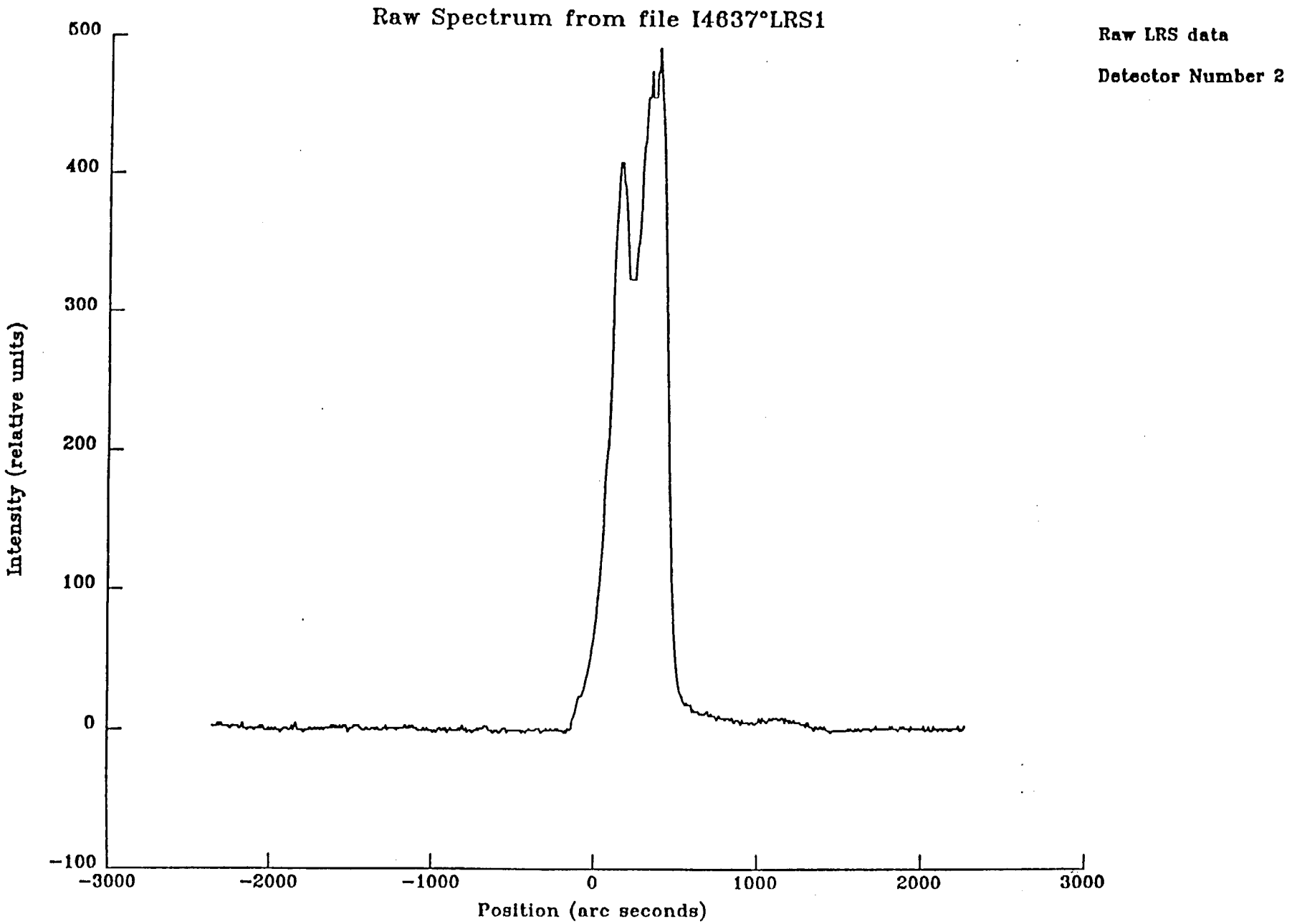


Figure 2c

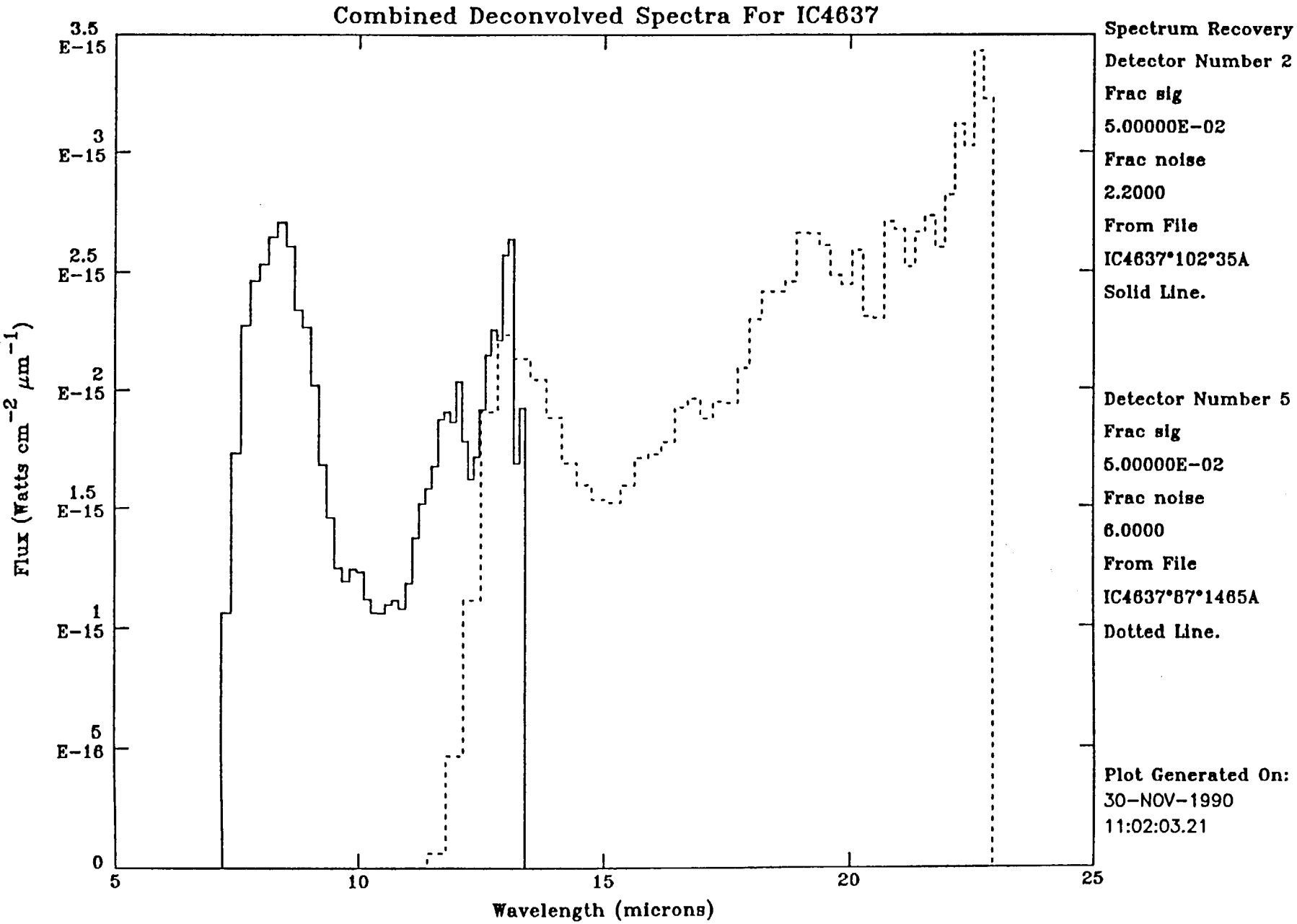
Combined Deconvolved Spectra For IC4637
Flux (Watts cm$^{-2}$ $\mu$m$^{-1}$)
3.5 E-15
3 E-15
2.5 E-15
2 E-15
1.5 E-15
1 E-15
5 E-16
0
5
10
15
20
25
Wavelength (microns)
Spectrum Recovery
Detector Number 2
Frac sig
5.00000E-02
Frac noise
2.2000
From File
IC4637°102°35A
Solid Line.
Detector Number 5
Frac sig
5.00000E-02
Frac noise
6.0000
From File
IC4637°87°1465A
Dotted Line.
Plot Generated On:
30-NOV-1990
11:02:03.21

Figure 2d

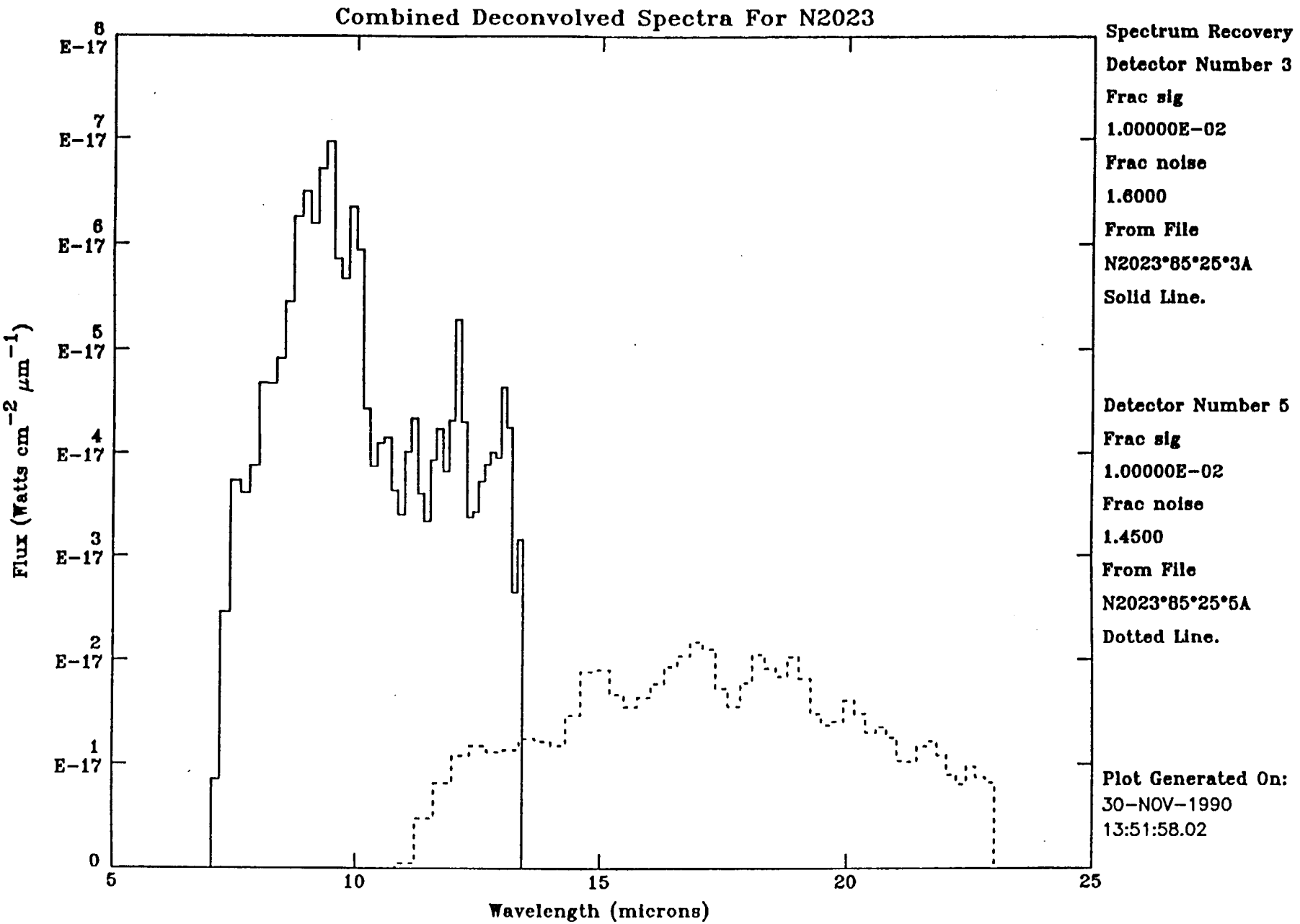
Combined Deconvolved Spectra For N2023
Flux (Watts cm$^{-2}$ $\mu$m$^{-1}$)
8 E-17
7 E-17
6 E-17
5 E-17
4 E-17
3 E-17
2 E-17
1 E-17
0
5
10
15
20
25
Wavelength (microns)
Spectrum Recovery
Detector Number 3
Frac sig
1.00000E-02
Frac noise
1.6000
From File
N2023°85°25°3A
Solid Line.
Detector Number 5
Frac sig
1.00000E-02
Frac noise
1.4500
From File
N2023°85°25°5A
Dotted Line.
Plot Generated On:
30-NOV-1990
13:51:58.02

Figure 3

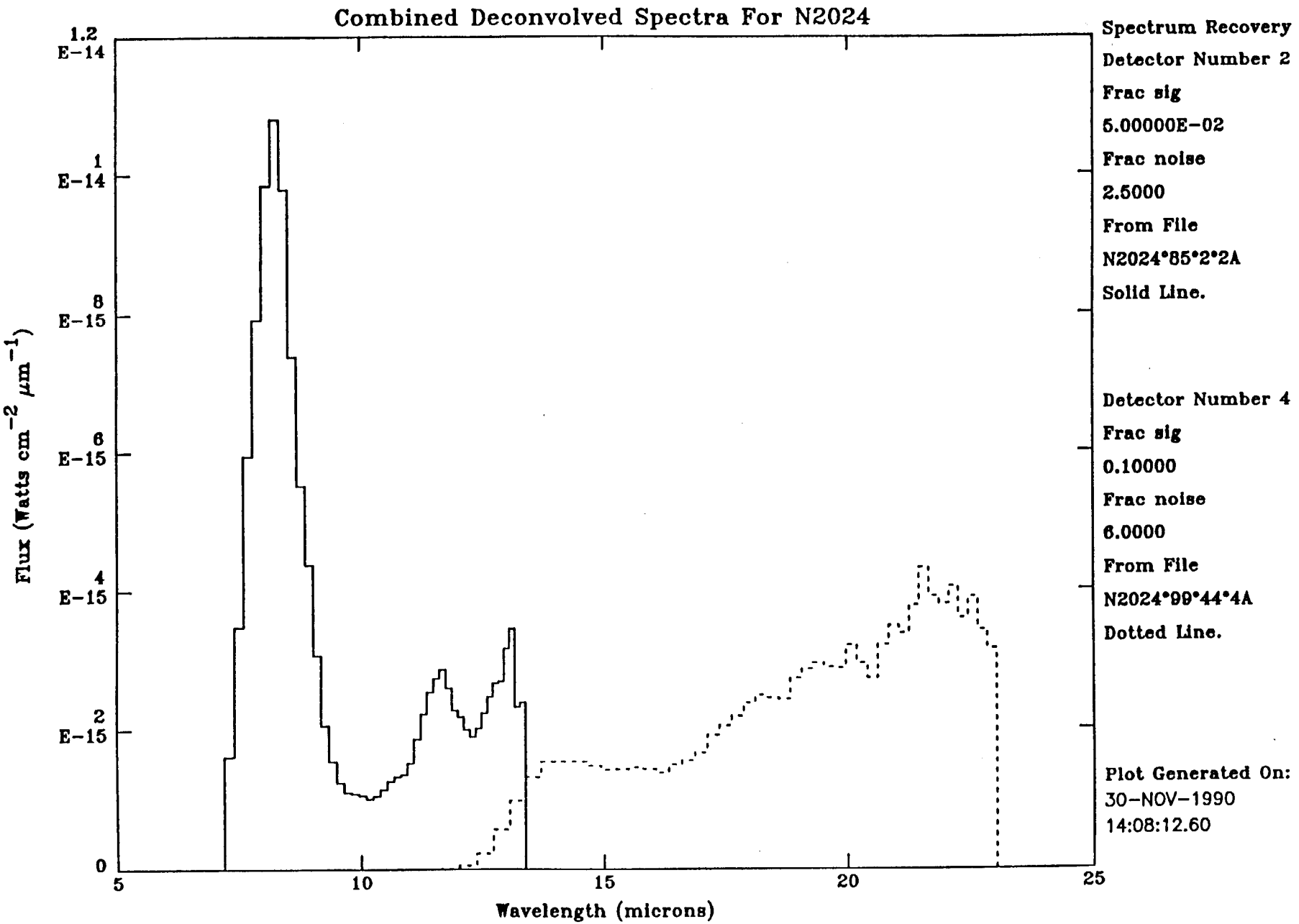
Combined Deconvolved Spectra For N2024
1.2 E-14
1 E-14
8 E-15
6 E-15
4 E-15
2 E-15
0
Flux (Watts cm$^{-2}$ μm$^{-1}$)
5
10
15
20
25
Wavelength (microns)
Spectrum Recovery
Detector Number 2
Frac sig
5.00000E-02
Frac noise
2.5000
From File
N2024*85*2*2A
Solid Line.
Detector Number 4
Frac sig
0.10000
Frac noise
6.0000
From File
N2024*99*44*4A
Dotted Line.
Plot Generated On:
30-NOV-1990
14:08:12.60

Figure 4

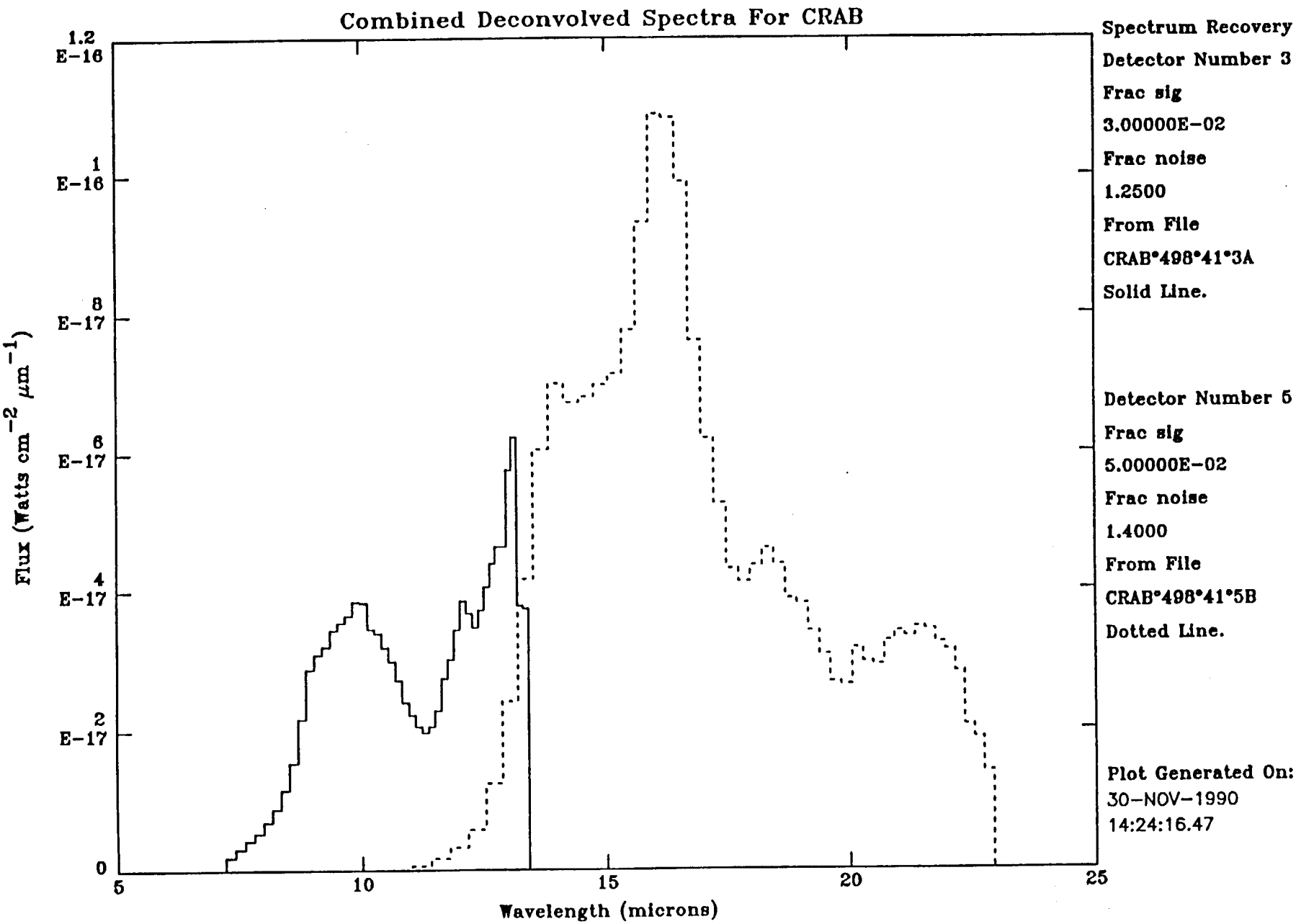
Combined Deconvolved Spectra For CRAB
1.2 E-16
1 E-16
8 E-17
6 E-17
4 E-17
2 E-17
0
Flux (Watts cm$^{-2}$ $\mu$m$^{-1}$)
5
10
15
20
25
Wavelength (microns)
Spectrum Recovery
Detector Number 3
Frac sig
3.00000E-02
Frac noise
1.2500
From File
CRAB°498°41°3A
Solid Line.
Detector Number 5
Frac sig
5.00000E-02
Frac noise
1.4000
From File
CRAB°498°41°5B
Dotted Line.
Plot Generated On:
30-NOV-1990
14:24:16.47

Figure 5